THE UNIVER ITY OF READING
DEPARTMENT OF MATHEMATIC

Development of Linear Models for Data Assimilation in Numerical Weather Prediction

by

Amo S. Lawl

Thesis submitted for the degree of
Doctor of Philosophy

May 2001

Abstract

Four-dimensional variational data assimilation requires the development of a discrete linear model with which to predict the evolution of a perturbation to the initial state of a nonlinear system. There are two ways in which this linear model may be derived. Beginning with the continuous nonlinear equations we may first discretize them and then linearize the numerical scheme thus formed, or we may first linearize the continuous equations and then apply some suitable discretization. In this thesis we compare these two methods.

Using simple models of an OD and a PD problem we show how the two methods may lead to models with different stability and accuracy characteristics. An important factor in determining the accuracy of the second method is found to be the representation of the background trajectory around which the model is linearized. We find that natural approximations to this trajectory may not only reduce the accuracy of the overall scheme but, within the context of semi-Lagrangian advection, may lead to a scheme which is no longer consistent.

As part of our analysis we identify a difficulty in testing the linear model formed by first linearizing and then discretizing. In order to overcome this we propose a new method for testing such models, which we demonstrate both theoretically and numerically.

Finally we consider the implementation of these ideas for operational weather forecasting, by developing the linearization of a three-dimensional weather forecasting model. For this case only the linear model formed by first linearizing and then discretizing is found. Numerical tests are performed using this model and the results interpreted in the light of the analysis of the simple problems.

Acknowledgements

My first acknowledgement is to my academic supervisor, Prof Nancy Nichols. I am extremely grateful for the careful attention she has given to this work and for her patience in explaining the finer mathematical points which I often overlooked. My gratitude goes also to my supervisor at the Met Office, Sue Ballard, for her constant support throughout this work, particularly for her help with the work on the three-dimensional model of Chapter 6 and for ensuring that I had sufficient time for this project.

I wish to thank Andrew Staniforth of the Met Office for his guidance in setting up the shallow water model of Chapter 5. My thanks go also to past and present members of the dynamics and data assimilation research and development groups at the Met Office, who have worked with me to build the model used in Chapter 6. I particularly acknowledge Mike Cullen who produced the initial design for this model.

I would like to thank my family, for their love and encouragement over many years. I also thank my friends who havonr59666g6jMetWM576djIWM52666jh7M54QQQSQj

I 6UwisQjd4Un6Uan82UWMQQ

Con en s

1 Introduction 6

2

5.4.4 Behaviour for large Courant number 129
5.5 Linearization state of PFM 132
5.6 stimating the tangent linear model error 140
5.7 Summary 144

6 Application to a Three-Dimensional Model **149**
6.1 The nonlinear model 150
6.1.1 The continuous equations 150
6.1.2 The discrete nonlinear model 153
6.2 The perturbation forecast model 155
6.2.1 The continuous equations 155
6.2.2 General formulation of the numerical scheme 157
6.2.3 Outline of the numerical scheme 159
6.2.4 Comments on the discretization 164
6.2.5 Details of the numerical scheme 166
6.3 Numerical experiments 172
6.3.1 Method 173
6.3.2 Correctness 177
6.3.3 rror measures 180
6.3.4 Perturbation fields 186
6.4 Linearization state 200
6.5 Summary 201

7 Conclusions and future work **204**
7.1 Summary of results 204
7.2 Further work 208

Appendices **211**

A Convergence of iterative procedure **211**

B Helmholtz equation for 3-dimensional model **216**

References **218**

is usually obtained from a previous short period forecast. The process of using the data to improve on this estimate is called *data assimilation*.

Until recently most methods of data assimilation have relied on a statistical combination of the data and background field. A review of such methods is given in [31] and [51]. A limitation of these methods is that they do not explicitly use the known model equations to constrain the problem in any way. This was changed by the proposal of the method of four-dimensional variational data assimilation (4D-Var) (e.g.

ment is not particular to 4D-Var, however, since the linearization of a nonlinear model is often used as a means of obtaining the adjoint model in other applications. Adjoin

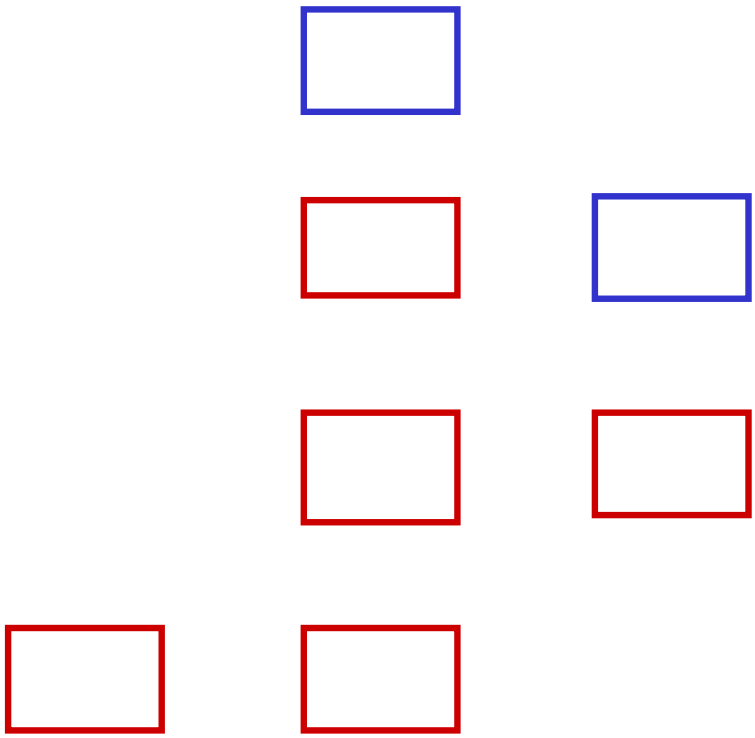

continuous nonlinear equations and linearize them, to form a set of continuous linear equations. These linear equations are then discretized using a suitable numerical scheme to form the discrete linear model, which we call a *perturbation forecast model* (PFM). The adjoint model can then be obtained from the perturbation forecast model in the same way as in Method 2 and so within the incremental 4D-Var scheme we still have the exact adjoint of our discrete linear model. We call this approach the *semi-continuous* method.

There are two main advantages to the semi-continuous method. The first is based on the premise that although the tangent linear model is valid for infinitesimal perturbations, what we actually want to model are finite perturbations of the size of uncertainties in the initial conditions [26]. The perturbation forecast model can be designed with this aim in mind. Thus it can be based on physical principles and can make some small approximations to the true tangent linear model. If the magnitude of such approximations is no greater than the error made by linearizing, then this should not affect the accuracy of the calculations, but will allow significant savings to be made to the running costs of the models. In fact, within the field of aerodynamics some attempt has been made to simplify the adjoint model to reduce its cost [60]. Our approach allows such simplifications to be made both in the equations of the linear model before any discretization by appealing to scale analysis and in the actual implementation of the numerical scheme.

A second advantage to this approach is that it is possible to avoid some of the problems which occur with numerical schemes which are difficult to linearize. Such difficulties will be reviewed in more detail in Section 3.2. For the present we note that one such problem can occur when deciding how to linearize an iterative scheme [64]. The semi-continuous method avoids this question by applying a suitable numerical scheme to the linearized equations.

In this thesis we do not treat the adjoint model, but concentrate our attention only on the discrete linear models formed by the discrete method (Method 2) and

the semi-continuous method (Method 3). We wish to compare the properties of the linear models formed in this way and to examine some of the issues which arise when these various methods

Chap er 2

Numerical me ho s or ifferen ial equa ions

In this chapter we review some of the concepts of numerical analysis and the numerical methods which we make use of in the remainder of the thesis. We begin in Section 2.1 by reviewing the analysis of initial value problems of ordinary differential equations (OD s) and then move on to partial differential equations (PD s) in Section 2.2. For each of these we review three essential properties of any numerical scheme, accuracy, convergence and stability. The accuracy of a numerical scheme is a measure of how well the numerical method approximates the original continuous equation. To measure this we introduce the definitions of the truncation error, order and consistency of a numerical scheme. However these only measure the error in the approximation of the equation and do not give information about how close the numerical solution is to the analytical solution. To obtain this we introduce the concept of convergence. Finally we have stability, which is a property of the discrete equations and makes no direct reference to the continuous problem. Stability together with consistency ensures that the numerical solution does not grow faster than the analytical solution. For most stability analyses we need to make some simplifying assumptions about the problem being solved. For example, the analysis is

Definition 2.1 *For the ODE problem (2.1), the global truncation error* $\boldsymbol{\tau}_n$ *of the scheme (2.2) at time* t_n *is defined by*

$$\boldsymbol{\tau}_n = \frac{\mathbf{y}(t_{n+1}) - \boldsymbol{\mathcal{F}}_n(\mathbf{y}(t_n), \Delta t)}{\Delta t}, \tag{2.3}$$

where $\mathbf{y}(t_n)$ *is the theoretical solution of the initial value problem (2.1).*

The global truncation error is often simply referred to as the truncation error and we will follow this henceforth. A Taylor series expansion of the truncation error in terms of the step size Δt allows us define the *order of accuracy* of the scheme ([44], p.225):

Definition 2.2 *The method (2.2) is said to have order* p *if* p *is the lowest integer for which*

$$\mathbf{y}(t_{n+1}) - \boldsymbol{\mathcal{F}}_n(\mathbf{y}(t_n), \Delta t) = O(\Delta t^{p+1}) \tag{2.4}$$

holds, where $\mathbf{y}(t_n)$ *is assumed to be a su ciently differentiable solution of the initial value problem (2.1).*

The requirement that the accuracy of the scheme increase as a smaller step size is used is then given by the property of *consistency*:

Definition 2.3 *The numerical method (2.2) is consistent if* $\boldsymbol{\tau}_n \to 0$ *as* $\Delta t \to 0$ *with* $n\Delta t$ *constant.*

This is equivalent to requiring that the order of the scheme be at least one.

2.1.2 Convergence

The convergence of a numerical scheme relates the analytical and numerical solutions. We first need to choose an appropriate norm to measure the distance between the solutions, which we write $\| \, . \, \|$. Commonly chosen norms for a vector $\mathbf{x} = \{x_j\}$ of length N are the maximum norm

$$\| \, \mathbf{x} \, \|_\infty = \max_{1 \le j \le N} |x_j| \tag{2.5}$$

and the uclidean, or l_2 norm

$$\| \mathbf{x} \|_2 = \left(\sum_{j=1}^{N} |x_j|^2 \right)^{\frac{1}{2}}. \tag{2.6}$$

We define the *global error* $\mathbf{e}_n$ of the numerical solution at time t_n by

$$\mathbf{e}_n = \mathbf{y}(n\Delta t) - \mathbf{y}_n. \tag{2.7}$$

Then we have:

Definition 2.4 *The numerical scheme (2.2) is a convergent approximation to the initial-value problem (2.1) if* $\| \mathbf{e}_n \| \to 0$ *as* $n \to \infty$ *with* $n\Delta t$ *constant.*

Convergence is related to consistency by means of the following theorem:

The2qq

Definition 2.5 *Let* $\boldsymbol{\delta}_n, \boldsymbol{\delta}_n^*$ *be any two perturbations of (2.2) and let* $\mathbf{z}_n, \mathbf{z}_n^*$ *be the resulting perturbed solutions for* $n = 0, 1, \ldots, M$. *Then if there exists constants* S *and* h_0 *such that, for all* $\Delta t \in (0, h_0]$,

$$\| \mathbf{z}_n - \mathbf{z}_n^* \| \leq S\epsilon \tag{2.10}$$

whenever

$$\| \boldsymbol{\delta}_0 - \boldsymbol{\delta}_0^* \| \leq \epsilon \tag{2.11}$$

for $0 \leq$

2.2 Partial differential equations

The partial differential equation problem we consider is the first order quasi-linear system in two independent variables

$$\frac{\partial \mathbf{u}}{\partial t} + \boldsymbol{F_1}(\mathbf{u}, x, t)\frac{\partial \mathbf{u}}{\partial x} + \boldsymbol{F_0}(\mathbf{u}, x, t) = 0, \tag{2.14}$$

where $\mathbf{u} = \mathbf{u}(x,t)$ is a real-valued vector, $t \in [0,T]$ and $x \in [0,L]$. The boundary conditions on x are periodic, so that $\mathbf{u}(0,t) = \mathbf{u}(L,t)$, and the initial condition $\mathbf{u}(x,0) = \mathbf{u_0}(x)$ is given. The partial derivatives of the vector $\mathbf{u}$ are defined to be the Jacobian of the vector with respect to the variable x or t. We interpret x as a spatial variable and t as a temporal variable. Many of the following results can easily be extended to more spatial dimensions by considering a vector $\mathbf{x} = [x_1, x_2, \ldots, x_k]$, but for the purposes of this chapter we restrict the discussion to one spatial dimension so as to simplify the notation.

In order to represent the numerical schemes we introduce step sizes $\Delta x, \Delta t$ for the independent variables x and t. Then at any spatial point x_i and time t_n the solution to the analytical system (2.14) is written $\mathbf{u}(x_i, t_n) = \mathbf{u}(i\Delta x, n\Delta t)$. The numerical approximation to this we write $\mathbf{u}_i^n$. We also need to define notation for the vector of values over all spatial points at a given time. We assume that we have N gridpoints, with $N\Delta x = L$, and define the vector of numerical solutions on the grid by

$$\mathbf{U}^n = [(\mathbf{u}_1^n)^T, (\mathbf{u}_2^n)^T, \ldots, (\mathbf{u}_N^n)^T]^T. \tag{2.15}$$

This is a numerical approximation to the analytical solution vector

$$\mathbf{U}(t_n) = [\mathbf{u}^T(x_1, t_n), \mathbf{u}^T(x_2, t_n), \ldots, \mathbf{u}^T(x_N, t_n)]^T. \tag{2.16}$$

We can then write a general one-step numerical method for solving the system (2.14) in the form

$$\mathbf{U}^{n+1} = \boldsymbol{\mathcal{G}}^n$$

Then we have:

Definition 2.10 *The numerical scheme (2.17) is a convergent approximation to the initial-value problem (2.14) in a given norm if* $\| \mathbf{e}_i^n \| \to 0$ *as* $n \to \infty, i \to \infty$ *with* $n\Delta t, i\Delta x$ *constant.*

2.2.3 Stability

In this section we restrict discussion to the stability of linear schemes for partial differential equations, that is schemes of the form (2.17) where $\boldsymbol{\mathcal{G}}^n$ is a linear function of $\mathbf{U}^n$. Then the stability of the numerical scheme (2.17) can be expressed by the following definition, taken from [42], p.30:

Definition 2.11 *The difference approximation (2.17) is stable in a given norm for a sequence* $\Delta t \to 0, \Delta x \to 0$ *if there are constants* α, K *such that for all* t_0, t_n *with* $t_n \geq t_0$ *and all* $\mathbf{U}^0$

$$\| \mathbf{U}^n \| \leq K e^{\alpha(t_n - t_0)} \| \mathbf{U}^0 \| . \tag{2.21}$$

For a PD problem, establishing the stability of a numerical system is an important part of demonstrating its convergence. The inherent link between these two properties is expressed by the *Lax equivalence theorem*:

Theorem 2.2 (Lax equivalence) *Given a properly posed initial-value problem and a finite-difference approximation to it that satisfies the consistency condition, stability is the necessary and sufficient condition for convergence, assuming that all conditions hold in the same norm. ([71], p.45).*

However, in general it is difficult to determine a condition such as (2.21) for a variable coefficient problem and so we usually consider only the stability of a constant-coefficient linear system. In this case the numerical scheme (2.17) can be written

$$\mathbf{U}^{n+1} = \mathbf{C_0}(\Delta t, \Delta x)\mathbf{U}^n, \tag{2.22}$$

where $\mathbf{C_0}$ is a time invariant matrix. Assuming a relationship between Δx and Δt we can write such a system in the form

$$\mathbf{U}^{n+1} = \mathbf{C_1}(\Delta t)\mathbf{U}^n, \tag{2.23}$$

with $\mathbf{C_1}$ a time invariant matrix and $0 \leq n\Delta t \leq T$. Since $\mathbf{C_1}$ is time invariant we have $\mathbf{U}^n = [\mathbf{C_1}(\Delta t)]^n\mathbf{U}^0$. The matrix $\mathbf{C_1}$ is the *amplification matrix*. Then to determine the stability of the linear system (2.23) we use the result of Richtmyer and Morton, which limits how much a feature of the initial data can be amplified in the numerical procedure. This leads to the following:

TheorezDDq2UF

Theorem 2.4 (von Neumann condition) *A necessary condition for the linear system (2.23) to be stable is that there exists a constant K such that for each of the eigenvalues λ_i of the amplification matrix $\mathbf{C_1}$*

$$|\lambda_i| \leq 1 + K\Delta t. \tag{2.28}$$

Furthermore we find that if $\mathbf{C_1}$ is a normal matrix, then this condition is both necessary and su cient for stability ([71], p.70).

In practice we must determine how the n

where $\hat{\mathbf{C}}_\mathbf{0}$ is the discrete Fourier transform of the matrix $\mathbf{C}_\mathbf{0}$. This is an equation

Thus the imaginary part of ω determines the amplitude of the solution and so corresponds to the stability analysis of above, with the solution growing for $\omega_i < 0$. On the other hand the real part ω_r gives information about the phase-speed. The expression for ω_r in terms of the other variables is called the *discrete dispersion relation*. Then ω_r is the frequency of the numerical solution and the phase speed is given by $-\omega_r/k$.

The derivation of such a relation allows comparison with an equivalent expression for the analytical system. We consider the linear analytical equations with constant coefficients. Then substituting Fourier modes of the form

$$\mathbf{u}(x,t) = \mathbf{u_0} e^{i(kx+\omega t)}, \tag{2.36}$$

with $\mathbf{u_0}$ constant in space and time, we can derive an expression for the frequency ω in terms of the wave number k. This analytical expression can be compared with the discrete dispersion relation to determine the change in frequency of a given Fourier mode caused by the numerical scheme. Th

2.3 Methods for ODE problems

In this section we restrict our attention to the scalar OD problem

$$\frac{dy}{dt} - f(y,t) = 0, \tag{2.37}$$

with $t \in [0,T]$ and $y(0) = y_0$. We define two types of numerical scheme for use in later chapters, linear multistep methods and Runge-Kutta methods.

Linear multistep methods for the solution of OD problems do not follow the general form of the scheme (2.2). We treat these methods only briefly in Chapter 4 and so the definition is included here only for completeness. The general *linear k-step method* for solving (2.37) is written (following [44], p.11),

$$\sum_{j=0}^{k} \alpha_j y_{n+j} = \Delta t \sum_{j=0}^{k} \beta_j f_{n+j}, \tag{2.38}$$

where α_j and β_j are constants and $f_n \equiv f(y_n, t_n)$. It is assumed that $\alpha_k \neq 0$ and that α_0 and β_0 are not both zero. Since the coefficients are arbitrary to the extent of a constant multiplier we assume that $\alpha_k = 1$.

These methods achieve high order accuracy by using function values at several steps in a linear scheme. In order to achieve higher order while retaining a one-step scheme it is necessary to allow nonlinearities to be introduced. This is the idea behind Runge-Kutta schemes. Following [44], p.114, we write a general *R-stage Runge-Kutta method* as

$$y_{n+1} - y_n = \Delta t \phi(y_n, t_n, \Delta t), \tag{2.39}$$

where

$$\phi(y_n, t_n, \Delta t) = \sum_{r=1}^{R} c_r k_r, \tag{2.40}$$

with

$$\sum_{r=1}^{R} c_r = 1 \tag{2.41}$$

and the functions k_r defined such that (2.39) satisfies the original differential equation (2.37) to the required order of accuracy. We note that the scheme (2.39) is of the general form of a one-step method (2.2) and so the theory developed in Section 2.1 is applicable to such schemes. The so-called 'classical' Runge-Kutta methods are derived by setting

$$\begin{aligned} k_1 &= f(y_n, t_n), \\ k_r &= f(y_n + \Delta t \sum_{s=1}^{r-1} b_{rs} k_s, t_n + a_r \Delta t), \\ a_r &= \sum_{s=1}^{r-1} b_{rs}, \\ & r = 2, 3, \ldots, R. \end{aligned} \tag{2.42}$$

A scheme with a given order of accuracy can then be designed by the appropriate choice of the coefficients a_r, b_{rs}, c_r. In Chapter 4 we will make use only of the two-stage Runge-Kutta method defined by choosing $b_{21} = 1$ and c_1

of the use of semi-Lagrangian schemes in atmospheric models is given in [79]. We begin with semi-Lagrangian advection in the context of a passive advection equation and then show how this is extended to treat the forced advection problem.

Following [79] we first illustrate the principle of semi-Lagrangian advection by considering the passive advection equation in one dimension. Thus we have

$$\frac{D\theta}{Dt} \equiv \frac{\partial \theta}{\partial t} + U(x,t)\frac{\partial \theta}{\partial x} = 0, \tag{2.44}$$

where θ is a scalar function being advected and

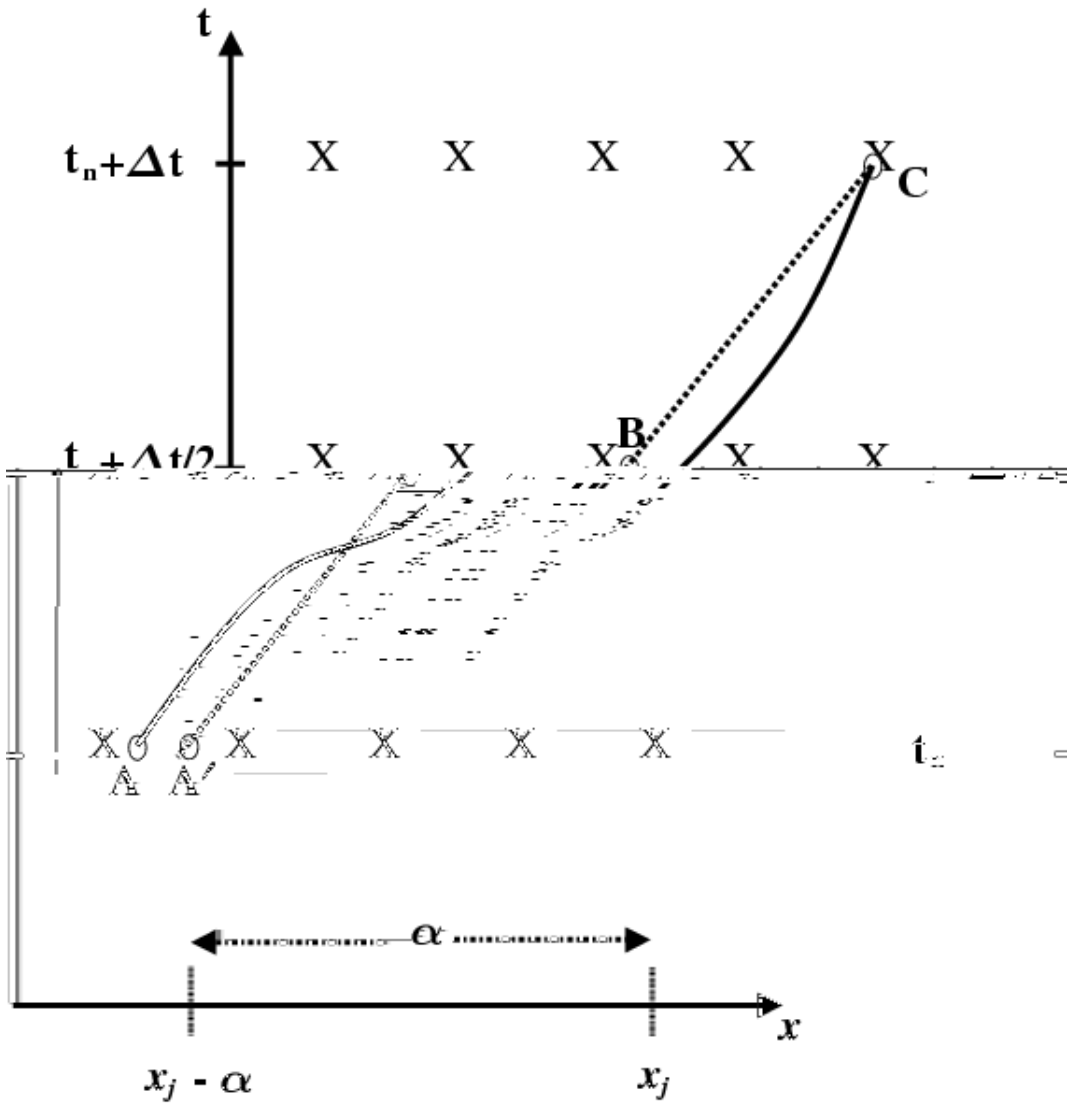

Figure 2.1: A schematic representation of two-time-level semi-Lagrangian advection.

Pudykiewicz et al. [66] proved that this iteration will converge provided that

$$\Delta t \max \left| \frac{\partial U}{\partial x} \right| < 1 \tag{2.50}$$

for this one-dimensional case. We note that the use of this iteration introduces values of the wind at time level $n-1$ into the scheme and so the scheme is not exactly a one-step scheme. However for most purposes of analysis we can consider the determination of the displacement separately and still consider the rest of the scheme as if it were jstilT[Tthexxhne-step.

The calculation of U^* requires values to be calculated at p ts which do not necessarily lie on the grid. Thus an interpostillationust be made using values at surrounding grid p

y considerations, the semi-Lagrangian method thus allows the time step to be chosen on the basis of accuracy considerations. However, in order to obtain the be from using larger time steps, it is imp t that iteration (2.47) be solved to at least $O(\Delta t^2)$ accuracy in to a void degrading the accuracy of the scheme as a whole [54].w o found toe sufficien t t o a hieve this

In later chapters we look at the linearizations of models using the schemes introduced in this section. First we review some of the work which has already been published on linear models.

Chap er 3

Developmen an es ing o linear mo els

In the previous chapter we introduced some concepts of numerical analysis and also some of the numerical schemes that we wish to use in this thesis. The theory of numerical analysis can be used not only to study the nonlinear model, but also to compare the linear models formed by the discrete method (the tangent linear model) and the semi-continuous method (the perturbation forecast model). The definitions of the previous chapter allow us to assess the properties of these discrete models and also compare them with the linear continuous system. In the present chapter we consider work directly concerned with the development and testing of linear models. We begin in Section 3.1 by looking at an alternative way in which tangent linear models have been assessed, by comparison with the discrete nonlinear model. Then, in Section 3.2, we review some previous studies which have looked at the properties of linear models. Finally, in Section 3.3, we propose a new method for evaluating a perturbation forecast model.

3.1 Comparison with discrete nonlinear model

3.1.1 Theory

In the meteorological literature the usual method of testing a tangent linear model follows that of Rabier and Courtier [67], which compares the evolution of a perturbation in the discrete linear model with the evolution of the same perturbation in the discrete nonlinear model. The method is based on a T

$\mathbf{U^0} + \alpha\boldsymbol{\delta}\mathbf{U^0}$. Then at any time t_n the difference between the two model runs is the perturbation $\boldsymbol{N}^n[\alpha\boldsymbol{\delta}\mathbf{U^0}]$ evolved in the nonlinear model, given by

$$\boldsymbol{N}^n[\alpha\alpha$$

the state defined by the trajectory $\boldsymbol{S}(t_n, t_0, \mathbf{U^0})$ and acting on the perturbation $\alpha\boldsymbol{\delta}\mathbf{U^0}$. Such a comparison enables us to understand how well the tangent linear model represents the true evolution of a perturbation in the discrete nonlinear model. The trajectory around which the tangent linear model is linearized is referred to as the *linearization state*. An important component of these experiments is the choice of the initial $\mathbf{U^0}$ used to generate this linearization state and of the initial perturbation $\alpha\boldsymbol{\delta}\mathbf{U^0}$. However, since these will depend on which particular model we are using, we leave discussion of this to the sections on numerical experiments in later chapters.

Within this thesis we wish to apply this test not only to the tangent linear model, but also to the linear model formed by discretizing the continuous linear equations, the perturbation forecast model. Thus we introduce the notation $\mathbf{L}(t_n, t_0)$ to mean the solution operator of a linear model formed by either discretizing first and then linearizing, or linearizing first and then discretizing. In the case where we linearize the discrete nonlinear model we have the tangen $\mathbf{L}($

Definition 3.1 *The linearization error* $\mathbf{E}^n$ *at time* t_n *is the difference between the nonlinear and linear variations. Thus*

$$\mathbf{E}^n = \boldsymbol{\mathcal{N}}^n[\alpha\boldsymbol{\delta}\mathbf{U}^\mathbf{0}] - \mathbf{L}(t_n, t_0)\alpha\boldsymbol{\delta}\mathbf{U}^\mathbf{0}. \tag{3.13}$$

Then the concept of correctness refers to whether the linear model represents the linear part of the nonlinear evolution. This is an objective property of a given discrete model and does not depend on the particular linearization state or initial perturbation. Thus following [65] we have

Definition 3.2 *The linear model* $\mathbf{L}(t_n, t_0)$ *is correct for any time* t_n *if*

$$\mathbf{L}(t_n, t_0) = \prod_{k=0}^{n-1} \left.\frac{\partial \boldsymbol{\mathcal{G}}^k}{\partial \mathbf{U}}\right|_{\mathbf{U}^k}. \tag{3.14}$$

Thus a correct linear model differs from the nonlinear model only in terms which are second order or higher. This allows us to formulate a necessary and sufficient condition for correctness as follows:

Lemma 3.1 *The linear model* $\mathbf{L}(t_n, t_0)$ *is correct if and only if for all initial perturbation directions* $\boldsymbol{\delta}\mathbf{U}^\mathbf{0}$

$$\lim_{\alpha \to 0} \frac{\| \mathbf{E}^n \|}{|\alpha|} = 0. \tag{3.15}$$

However we note that although Lemma 3.1 allows us to test for correctness by considering the limit of small perturbations, the concept of correctness is not itself dependent on the perturbation size.

Validity on the other hand is a more subjective property, since it is a judgement as to how well the linear variation approximates the nonlinear variation. This depends on the particular value of the linearization state and perturbation being used. The judgement as to whether a linear model is valid in a given situation will also depend somewhat on the application for which the model is required. We use the concepts of [65] to define validity as follows:

Definition 3.3 *The linear model* $\mathbf{L}(t_n, t_0)$ *is valid at time* t_n *for a given background trajectory* $\boldsymbol{S}(t_n, t_0, \mathbf{U^0})$ *and initial perturbation* $\alpha\boldsymbol{\delta}\mathbf{U^0}$ *if*

$$\| \mathbf{E}^n \| \ll \| (\alpha\boldsymbol{\delta}\mathbf{U^n})^L \| . \tag{3.16}$$

More discussion of the choice of norm is made in Section 3.1.2. This definition is equivalent to the requirement that the true nonlinear evolution of a given finite perturbation be dominated by the part of the evolution predicted by the linear model.

For the purpose of comparing the two different methods for deriving the linear model, we note that in general only the tangent linear model will be correct according to Definition 3.2 of correctness. However, since for most applications we are concerned with predicting the evolution of a finite perturbation in a given situation, it is the validity of the linear model which is most of interest. In the following chapters therefore we concern ourselves more with comparing the validity of the tangent linear and perturbation forecast models, though some discussion of correctness will be made. We now consider some of the ways in which correctness and validity can be determined in practice.

3.1.2 Quantifying the error

Using the above notation we hav

is reasonably linear and so the tangent linear approximation is valid. A high relative error on the other hand indicates that nonlinear effects are having a big influence on the evolution. For the perturbation forecast model the relative error is dependent on a combination of the nonlinearity of the evolution and the closeness of the discrete scheme to the tangent linear model. For a given situation it gives information as to how well the linear model approximates the nonlinear evolution, taking into account both of these effects.

As we have already mentioned, an important component of this measure is the definition of the norm. In [67] Rabier and Courtier choose an energy based norm. Such a norm has the advantage of being physically and mathematically meaningful, since it is weighted by the grid box area and so the discrete norm converges to the corresponding continuous norm as the grid size is reduced. In this way we do not give too much weight to polar points on a regular latitude-longitude grid. However, when we are testing a model for correctness (or near correctness for a perturbation forecast model) it may be more desirable to give equal weight to all grid points, to ensure that any problems near the poles show up immediately. In this case the root mean square (rms) value may be a more useful norm. This norm is defined for a vector $\mathbf{x} = \{x_j\}$ of length N by the formula

$$rms(\mathbf{x}) = \left(\frac{1}{N} \sum_{i=1}^{N} x_i^2 \right)^{\frac{1}{2}}. \tag{3.21}$$

The root mean square norm is simply the l_2 norm (2.6) scaled by the square root of the length of the vector. We note that in spherical geometry this norm does not converge to a continuous norm as the grid size is reduced. Vukićević and Bao [88] use this norm for their experiments. They measure the total error with respect to the size of the nonlinear perturbation rather than the linear perturbation, defining the *solution error* E_S by

$$E_S = 100 \frac{rms(\boldsymbol{N}^n[\alpha \boldsymbol{\delta} \mathbf{U_0}] - \mathbf{L}(t_n, t_0)[\alpha \boldsymbol{\delta} \mathbf{U_0}])}{rms(\boldsymbol{N}^n[\alpha \boldsymbol{\delta} \mathbf{U_0}])}. \tag{3.22}$$

A final measure of the difference between the linear and nonlinear perturbations is the correlation coefficient, used for example by rrico et al. [28]. If we have two vectors of length N, $\mathbf{x} = \{x_j\}$ and $\mathbf{y} = \{y_j\}$, then we define the correlation coefficient $C[\mathbf{x}, \mathbf{y}]$ between $\mathbf{x}$ and $\mathbf{y}$ by

$$C[\mathbf{x}, \mathbf{y}] = \frac{\sum_{i=1}^{N}(x_i - \bar{x})(y_i - \bar{y})}{\left(\sum_{i=1}^{N}(x_i - \bar{x})^2 \sum_{i=1}^{N}(y_i - \bar{y})^2\right)^{\frac{1}{2}}}, \tag{3.23}$$

where

$$\bar{x} = \frac{1}{N} \sum_{i=1}^{N} x_i,$$

$$\bar{y} = \frac{1}{\quad}$$

0.0

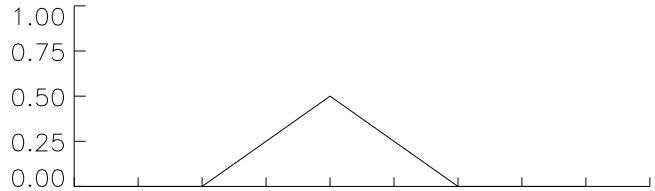

Figure 3.4: Linearization error for perturbation of Figure 3.2

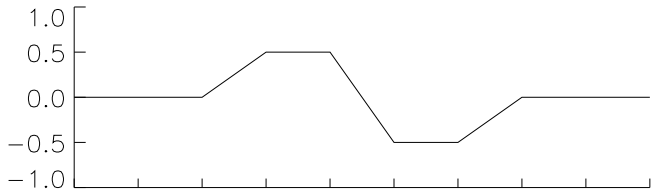

Figure 3.5: Linearization error for perturbation of Figure 3.3

valid primarily for perturbations of meteorological significance and so a subjective assessment of the perturbation fields is also useful.

So far we have seen essentially two differen

is inherently linked to that of the linear model [28]. In fact the tangent linear model could be found by taking the adjoint of the adjoint model formed by the continuous method. We first look at the work which has concentrated solely on the tangent linear model.

Studies of the properties of the direct linearization of a discrete nonlinear model have been made within meteorology and within the more general field of automatic differentiation (AD), but surprisingly the interaction between the two has been very limited. Certainly meteorologists have made use of the techniques of AD in deriving linear and adjoint models (e.g. [14], [93]), but little reference is made to the theoretical results of AD in the meteorological literature. A particular example of this is the study of the linearization of iterative processes. These are important in meteorological models, particularly when semi-implicit semi-Lagrangian schemes are used. These schemes contain iterative processes within the departure point calculation of the semi-Lagrangian scheme and in the solution of the elliptic pressure equation which arises from the implicitly treated terms. Within the meteorological literature the problem of linearizing such processes has been studied by Polavarapu and Tanguay [64]. They examine the direct linearization of each step of a fixed-point iterative procedure and also an approximation to this which does not vary the linearization state from iteration to iteration. They establish that the direct linearization converges more slowly than the nonlinear reference iteration. This problem has also been looked at in detail within the field of AD and studies therein have looked at the theoretical properties of some simplifications [35], [4].

Another area of difficulty which has been studied in the context of meteorological tangent linear models is the treatment of interpolation, which is an important part of semi-Lagrangian schemes. As we saw in our review of such schemes in Section 2.4, the values of a field at the departure point must be found by interpolation from the values at surrounding grid points. In order to calculate which are the nearest grid points it is necessary to calculate the nearest integer value to the departure

point displacement from the coordinate origin. In Fortran this is provided by the intrinsic function INT. However, this process is non-differen

the areas where the linearization error was highest. However they conclude that in practice this problem was unlikely to cause errors larger than those associated with other approximations within the data assimilation system.

A second method of treating the problem of discontinuous processes within physical parametrizations is to redesign the nonlinear schemes such that these discontinuities do not occur ([2], [94], [90]). At CMWF and Meteo-France this path has been pursued and a simplified set of nonlinear physical parametrizations has been developed for use in the incremental 4D-Var scheme [41]. They have been designed in such a way that their linearizations and adjoints are straightforward to obtain. However, the original physical parametrizations are used in the calculation of the nonlinear trajectory.

At this point we highlight one of the benefits of the semi-continuous approach to forming the linear model. Since we work from the continuous linear equations, we hav

derive a perturbation forecast model, rather than linearizing the discrete numerical schemes.

In the published studies on adjoint models, there have been various comparisons made of the adjoint model formed by the continuous and the discrete methods, but no work on the adjoint model formed by the semi-continuous method. Although the continuous method is not of great interest for the application of incremental 4D-Var, since it does not provide a discrete linear model directly, some of the results of these studies are relevant to the present argument and so we review these here.

One important area which has been studied is the adjoints of advection schemes. Sirkes and Tziperman [76] demonstrated that the adjoint of a leapfrog scheme formed using the discrete method shows a sensitivity to a computational mode which does not appear when the adjoint is formed by the continuous method. This occurs because the adjoint formed by the discrete method gives a sensitivity with respect to the discrete numerical model, of which the leapfrog computational mode is an important component. On the other hand, the adjoint formed by the continuous method approximates a sensitivity with respect to the continuous system. Although the authors conclude that both adjoints are valid if only a gradient at the initial time is needed, as is true for incremental 4D-Var, they do state that this is symptomatic of a wider problem of ensuring the stability of an adjoint model.

More recently Thuburn and Haine [87] investigated the adjoints of nonoscillatory advection schemes. Such schemes, in order to be monotone and better than first-order accurate, are necessarily nonlinear. The authors show that for a large class of such schemes the sensitivities calculated using the discrete adjoint do not agree with those calculated from a direct perturbation of the forward model. Moreover they prove that the discontinuities in the advection schemes cannot be smoothed out in some way to prevent this without sacrificing some desirable properties of the schemes.

A comparison of the continuous and discrete approaches to adjoints in the context

the linear model formed by linearizing the discrete scheme, the tangent linear model. We now propose a new method designed to evaluate the accuracy of a perturbation forecast model.

3.3 Comparison with estimated tangent linear model error

One of the difficulties in testing a perturbation forecast model which we referred to in Section 3.1.2 is the fact that the linearization error does not tend to zero as a perturbation becomes infinitesimally small. For experiments with finite size perturbations it would be useful to know how much of the linearization error we do see is due to nonlinear effects and how much is due to the fact of using a perturbation forecast model instead of a tangent linear model. In this section we develop a new method of assessing this, which uses the nonlinear model to estimate the linearization error that we would obtain if we had a tangent linear model. This can then be compared with the actual linearization error from the perturbation forecast model.

We consider our discrete nonlinear model to be of the form (3.3). In order to derive our formula for the estimate of the linearization error we first need to expand the nonlinear model using a Taylor series. To do this we follow [67]. We assume that the vector $\mathbf{U}$ is represented by p components U_l and that the model $\boldsymbol{S}$ is represented by p scalar components S_l with $l = 1, \ldots, p$, so that

$$U_l^n = S_l(t_n, t_0, \mathbf{U^0}). \tag{3.26}$$

Then from [67] we have the expansion

$$\begin{aligned} S_l(t_n, t_0, \mathbf{U^0} + \boldsymbol{\delta}\mathbf{U^0}) &= S_l(t_n, t_0, \mathbf{U^0}) \\ &+ \sum_{i=1}^{p} \frac{\partial S_l}{\partial U_i}(t_n, t_0, \mathbf{U^0})\delta U_i^0 \\ &+ \frac{1}{2!} \sum_{i=1}^{p} \sum_{j=1}^{p} \frac{\partial^2 S_l}{\partial U_i \partial U_j}(t_n, t_0, \mathbf{U^0})\delta U_i^0 \delta U_j^0 \\ &+ \frac{1}{3!} \sum_{i=1}^{p} \sum_{j=1}^{p} \sum_{k=1}^{p} \frac{\partial^3 S_l}{\partial U_i \partial U_j \partial U_k}(t_n, t_0, \mathbf{U^0})\delta U_i^0 \delta U_j^0 \delta U_k^0 \\ &+ h.o.t. \end{aligned} \tag{3.27}$$

We wish to use this Ta

(3.9). Then from (3.27) we see that $\mathbf{E}^n$ consists of the p components E_l^n given by

$$E_l^n = \frac{1}{}$$

Chap er 4

An ODE ini ial value problem

In this chapter we wish to investigate the principle of the semi-continuous method for developing a linear model by looking at a very simple problem. The results of this chapter we have also published separately in a technical report of the Met Office [46]. The problem we study is an initial value problem of a scalar ordinary differential equation. The aim of looking at this problem is to see in a simple context what kind of results we may expect in more complicated models.

We consider a general OD initial value problem for a scalar function $y(t)$ of the form

$$\frac{dy}{dt} = f(y), \quad t \in [0,T], \; y(0) = y_0, \tag{4.1}$$

where f is explicitly a function in y only. This is a scalar equation of the same form as the general equation (2.1) introduced in Section 2.1. The linearization of (4.1) is

$$\frac{d(\delta y)}{dt} = f'(y)\delta y, \tag{4.2}$$

where

$$f'(y) \equiv \frac{df}{}$$

coefficients from different time levels. In order to develop the linear model by the discrete method we apply a numerical scheme to equation (4.1) and then linearize this scheme. This gives the tangent linear model (TLM). We wish to compare this linear model with that derived by the semi-continuous method, that is by applying the original numerical scheme directly to equation (4.2). This second linear model is the perturbation forecast model (PFM). Within this chapter we compare the TLM and PFM for a particular numerical scheme, looking particularly at the properties of accuracy and stability.

Before we continue it is desirable to say something about the existence of solutions to these equations. We assume that f is continuous on some interval $[y_0, y_T]$ and satisfies a Lipschitz condition

$$\| f(y_1) - f(y_2) \| \leq L \ \| y_1 - y_2 \| \tag{4.4}$$

for all $y_1, y_2 \in [y_0, y_T]$. L is the Lipschitz constant. This ensures that (4.1) has a unique solution while y remains in the region $[y_0, y_T]$ ([30], section 1.1).

In order to show that the tangent linear problem (4.2) has a Lipschitz condition and therefore a unique solution, we first note that for given perturbations δy

4.1 Linear multistep methods

We consider the general linear k-step method as defined by (2.38) of Chapter 2. Applying such a scheme to (4.1), we have

$$\sum_{j=0}^{k} \alpha_j y_{n+j} = \Delta t \sum_{j=0}^{k} \beta_j f_{n+j}, \tag{4.7}$$

where $f_n \equiv f(y_n)$. A linearization of this scheme produces the tangent linear model

$$\sum_{j=0}^{k} \alpha_j \delta y_{n+j} = \Delta t \sum_{j=0}^{k} \beta_j f'_{n+j} \delta y_{n+j}. \tag{4.8}$$

It is clear that exactly the same result would be obtained by applying the original scheme (2.38) to the linear equation (4.2). Hence, for the case of a general linear multistep method, the discrete method and the semi-continuous method are equivalent.

4.2 Nonlinear methods

The conclusion of the previous section does not necessarily hold when we apply a nonlinear numerical method to the problem. To illustrate this, we use the example of a two-stage Runge-Kutta scheme defined by equation (2.43) of Chapter 2, which

For the nonlinear problem we are considering we note that the function f does not depend explicitly on t and therefore we have the scheme

$$\begin{aligned} k_1 &= f(y_n), \\ k_2 &= f(y_n + \Delta t\, f(y_n)), \\ y_{n+1} &= y_n + \frac{\Delta t}{2}(k_1 + k_2). \end{aligned} \tag{4.10}$$

Applying this scheme to the nonlinear equation (4.1) gives the discrete nonlinear model

$$y_{n+1} = y_n + \frac{\Delta t}{2}\left\{f(y_n) + f(y_n + \Delta t\, f(y_n))\right\}. \tag{4.11}$$

In order to form the TLM we linearize this scheme to obtain

$\delta y_{tt_{in}y}$ Δ

and linearization are not commutative. We note however that if we were to apply the Runge-Kutta scheme to the coupled system given by the continuous nonlinear equation (4.1) and the continuous linear equation (4.2), then the resulting linear model would be the same as the tangen

ships

$$\begin{aligned}
\frac{dy}{dt} &= f(y(t)), \\
\frac{d^2y}{dt^2} &= f(y(t))f'(y(t)), \\
\frac{d^3y}{dt^3} &= [f'(y(t))]^2 f(y(t)) + f''(y(t))[f(y(t))]^2,
\end{aligned}$$

we find that the truncation error is given by

$$\begin{aligned}
\tau_{NL} &= \left(\frac{1}{6}f(y(t_n))[f'(y(t_n))]^2 - \frac{1}{12}f''(y(t_n))[f(y(t_n))]^2\right)\Delta t^2 \\
&+ O(\Delta t^3). \qquad (4.16)
\end{aligned}$$

By this we see that the scheme is second order in time.

Now we wish to examine the truncation errors for the two linear models (4.12) and (4.14), which we denote τ_1 and τ_2 respectively. First we must be clear about what these quantities mean. The PFM (4.14) is a scheme written to approximate the linear equation (4.2) and so the truncation 5B thIe3S5:,,,)(4.1:Lhem5],]Bn=S5:,,,)r)II=e

last term of the equation around $f'(y(t_n))$. Then using the relationships

$$d(\delta y)$$

The linear model by the semi-continuous method is determined by applying the numerical scheme (4.9) to the analytical linear equation (4.24). This gives the PFM

$$\delta y_{n+1} = \delta y_n + y_n \Delta t \delta y_n + y_{n+1} \Delta$$

4.4 Numerical experiments

W

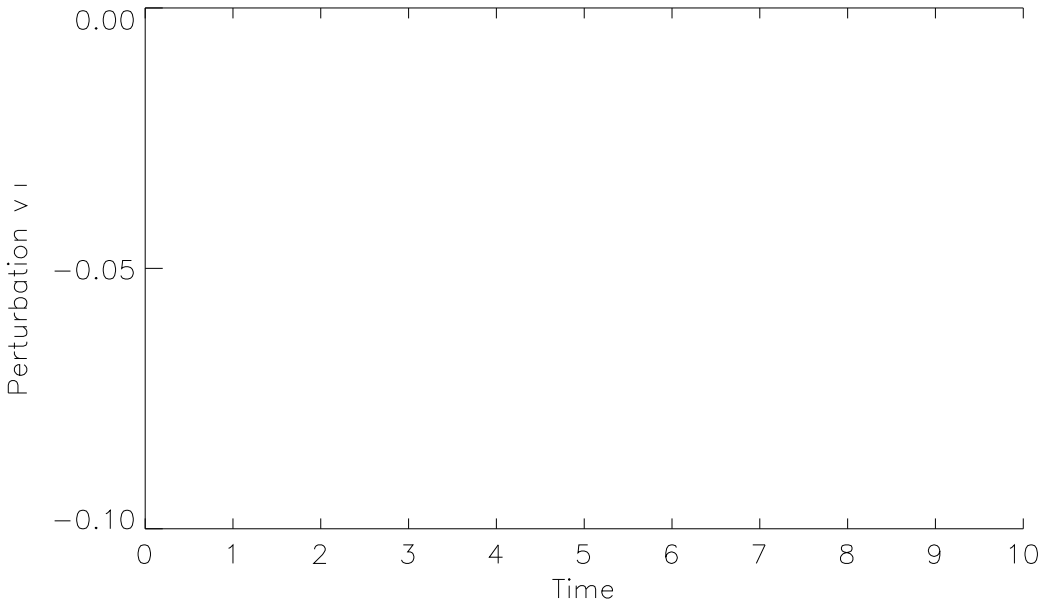
0.00
−0.05
−0.10
Perturbation v 1
0
1
2
3
4
5
6
7
8
9
10
Time

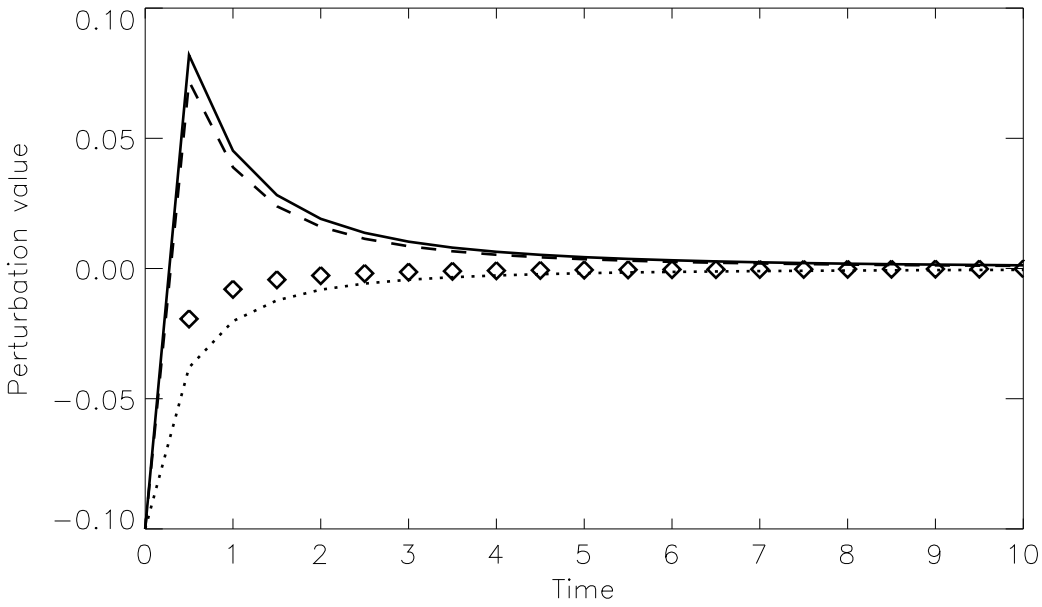

Figure 4.3: Plot of perturbation against time for $\Delta t = 0.5$. The solid line indicates the evolution in the nonlinear model, the dashed line shows the tangent linear model evolution, the dotted line shows the perturbation forecast model evolution and the diamonds indicate the true nonlinear variation.

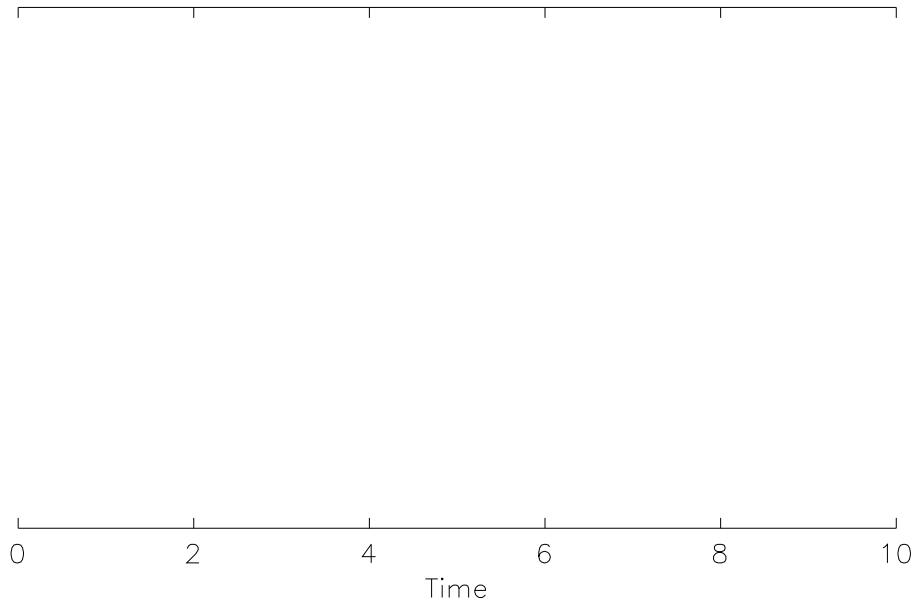
0
2
4
6
8
10
Time

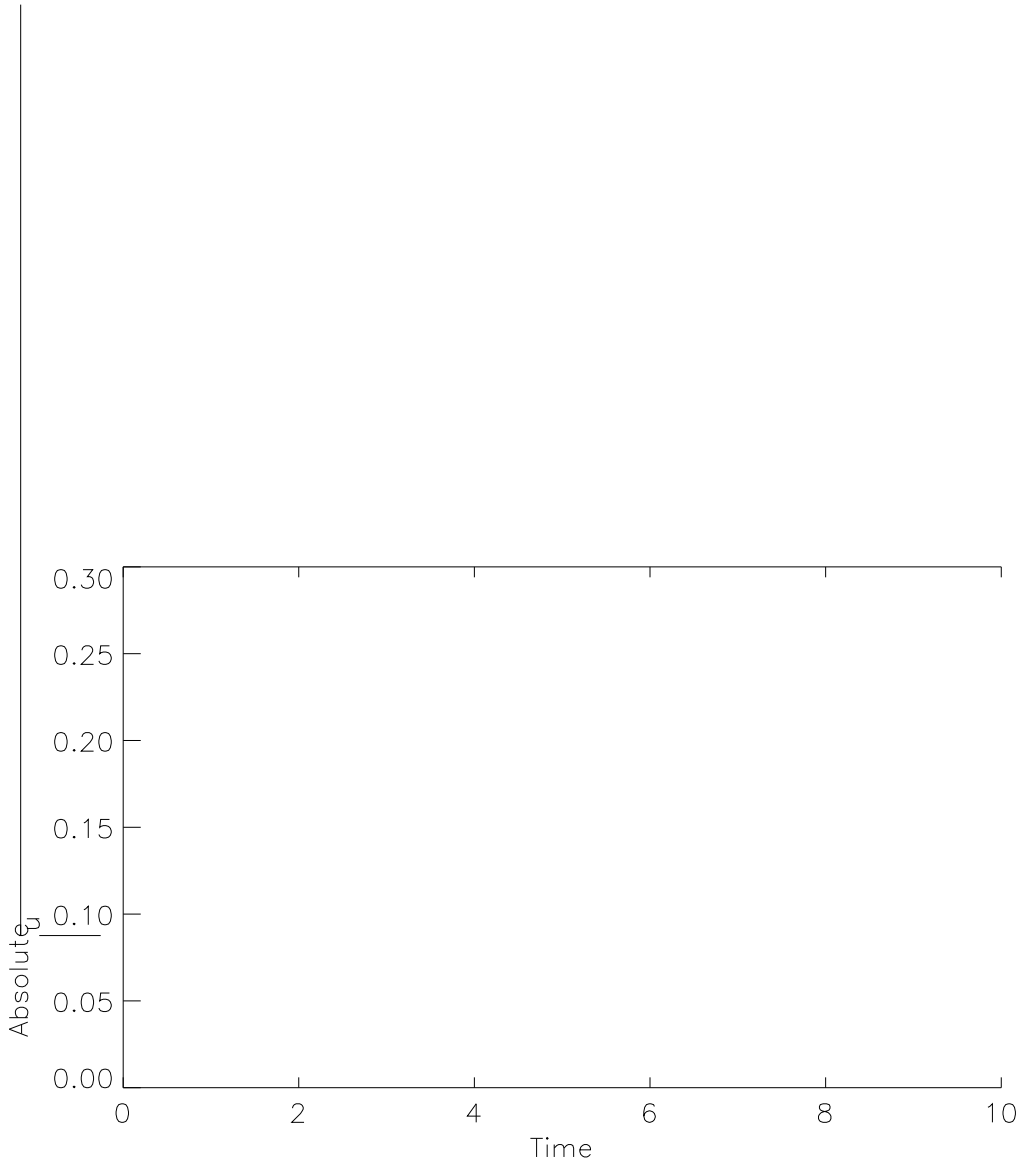
0.30
0.25
0.20
0.15
0.10
0.05
0.00
Absolute u
0
2
4
6
8
10
Time

analytical solution to the linear equation (4.25), we see also that δy at any time t is always a positive factor times the initial δy and thus cannot change sign. Hence the analytical solutions to both the nonlinear and linear problems tell us that an initial negative perturbation must remain negative throughout the model run. Thus the behaviour of the perturbation in the discrete nonlinear model is one which is not allowed by the analytical solution.

Turning now to the linear models, we wish to understand why the solution of the model formed by the discrete method (the dashed line in Figure 4.3) follows the erroneous nonlinear model solution. In particular, we wish to determine whether this is an effect of an incorrect linearization state or a feature of the scheme itself. The experiments were therefore repeated, using a time step of $\Delta t = 0.25$ in the nonlinear model run, and then using the linearization state from this to force the linear models with a time step of $\Delta t = 0.5$. The result of this is shown in Figure 4.6. From this experiment we see that a more correct linearization state is not enough to prevent the perturbation from changing sign in the linear model formed by the discrete method (the TLM). The linear model is unstable even though the nonlinear model is well-behaved. The problem must therefore be inherent in the scheme of the TLM. We therefore analyse further the linear schemes, to understand how their behaviour changes with time step.

4.4.1 Analysis of numerical results

We first consider the numerical stability of the schemes. To investigate the linear stability limit of the Runge-Kutta scheme (4.10) we follow the method of Section 2.1.3 and apply the scheme to the scalar system

$$\frac{dy}{dt} = \mu y, \qquad \mu < 0. \tag{4.33}$$

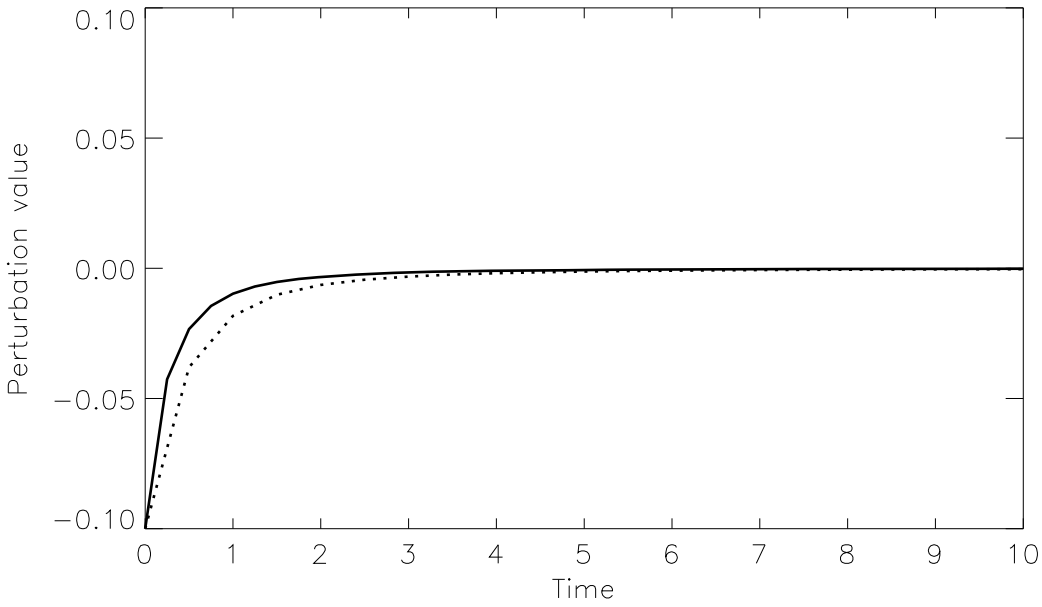
0.10
0.05
0.00
−0.05
−0.10
Perturbation value
0
1
2
3
4
5
6
7
8
9
10
Time

Then requiring that the modulus of the amplification factor be less than one, we find a limit on the time step Δt for this scheme of

$$\Delta t < -\frac{2}{\mu}. \tag{4.34}$$

Hence with μ set to $2y$, as in our linear equation (4.24), we find that for stability we require

$$\Delta t < -\frac{1}{y}. \tag{4.35}$$

For $y = -2.5$ this gives a time step limit of $\Delta t < 0.4$.

This limit also holds for the linear model formed by the discrete method (the TLM). The amplification factor λ_n of the linear scheme is given by

$$\lambda_n = \frac{\delta y_{n+1}}{\delta y_n}. \tag{4.36}$$

For an initial negative perturbation to remain negative we require that λ_n is always positive. A simple analysis of the TLM (4.28) sho

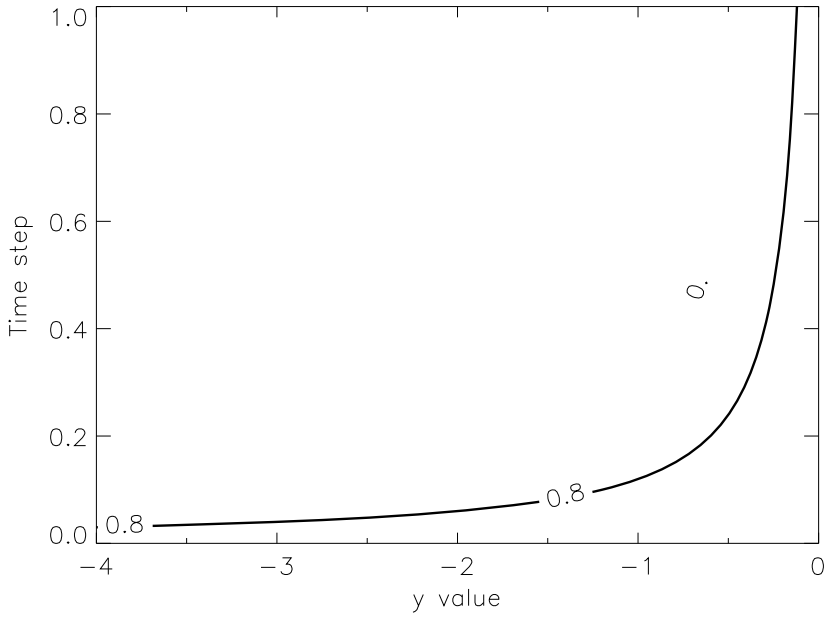
1.0
0.8
0.6
0.4
0.2
0.0
Time step
−4
−3
−2
−1
0
y value
0.8
0.8
0.

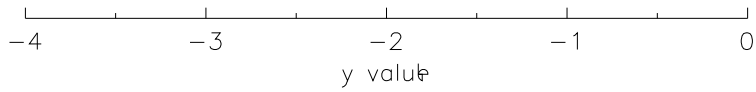
−4
−3
−2
−1
0
y value

of each scheme at time t_{n+1} by

$$E = \delta y(t_{n+1}) - \delta y_{n+1}, \tag{4.37}$$

where we assume $\delta y_n = \delta y(t_n)$ and $y_n = y(t_n)$. Then, expanding about time t_n we find the following local errors after one time step:

• for the discrete method (TLM)

$$E_1 = [2y(t_n)^3\Delta t^3 + 5y(t_n)^4\Delta t^4 + 6y(t_n)^5\Delta t^5 + O(y(t_n)^6\Delta t^6)]\delta y(t_n); \tag{4.38}$$

• for the semi-continuous method (PFM)

$$E_2 = [y(t_n)^3\Delta t^3 + \frac{5}{2}y(t_n)^4\Delta t^4 + 5y(t_n)^5\Delta t^5 + O(y(t_n)^6\Delta t^6)]\delta y(t_n). \tag{4.39}$$

The higher order terms of these errors are identical, and so we can write an exact expression for their difference,

$$E_1 - E_2 = [y(t_n)^3\Delta t^3 + \frac{5}{2}y(t_n)^4\Delta t^4 + y(t_n)^5\Delta t^5]\delta y(t_n). \tag{4.40}$$

A simple analysis shows that within the limits of stability, the magnitude of the error E_2 is greater than that of E_1 wherever

$$-1 < y\Delta t < -\frac{1}{2}. \tag{4.41}$$

For a value of $y = -2.5$ this corresponds to a time step range of $0.2 < \Delta t < 0.4$, and so explains the relative accuracy of the two linear solutions when $\Delta t = 0.35$. When the time step is less than 0.2, we find that the scheme formed by the semi-continuous method is more accurate.

4.5 Linearization state

Within each of the linear models we find a dependence on the linearization state $y(t)$ about which the model has been linearized. From equation (4.13) we note that

the intermediate values. An expansion of the truncation error finds that both of these options are second order accurate.

Although it may be argued that this is not a fair comparison, since by changing the time of the linearization state we are changing the numerical scheme, this is in fact what we do in practice. In the three-dimensional perturbation forecast model being developed at the Met Office, of which we speak in detail in Chapter 6, we apply the scheme of the nonlinear model to the linear equations, and afterwards decide where to take our linearization state. Hence it is important to know to what extent the choice of linearization state can affect the accuracy of the model.

To illustrate the effects of this choice we repeat the numerical experiment of the previous section using the stheme giLtr5Lciair

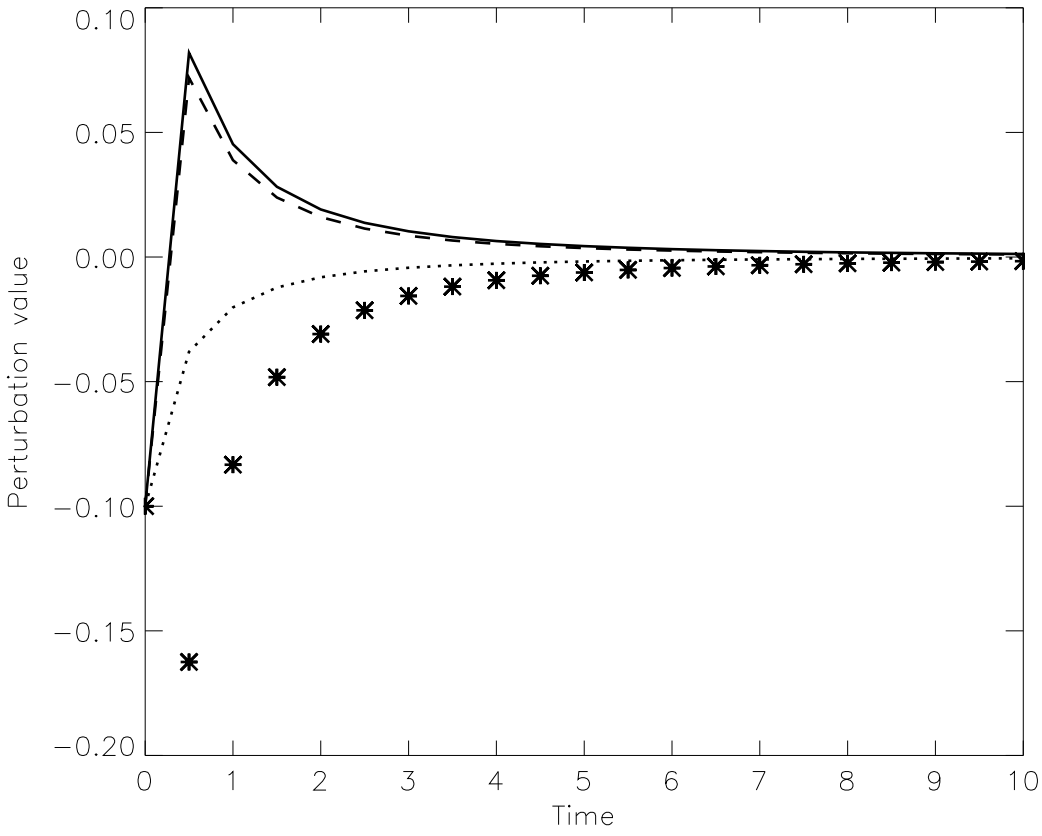
0.10
0.05
0.00
−0.05
−0.10
−0.15
−0.20
Perturbation value
0
1
2
3
4
5
6
7
8
9
10
Time

the linear stability limit of the discrete nonlinear model, whereas the perturbation forecast model allows larger time steps. Hence it is possible that the TLM may become unstable for time steps at which the PFM is still stable. Such a difference may be important if we wish to run the linear model at a lower temporal resolution than the nonlinear model. In practice this may be the case for incremental 4D-Var, since many iterations of the linear model will be required and means to reduce the cost of the linear model must therefore be sought. There may of course be situations in which the TLM is more stable than the PFM. However an advantage we see of the semi-continuous method is that the stability of the linear model may be better controlled *a priori* by careful choice of the numerical scheme used to discretize the linear equations.

For the numerical experiments in which both linear models remained stable, we find that the relative accuracy of the TLM and PFM compared with the analytical solution is dependent upon the value of the time step and the value of the linearization state. Thus it is not clear that either method holds an advantage over the other from an accuracy point of view.

A corollary of the results in this chapter is that testing the validity of the linear model must be performed with a good understanding of the nature of the numerical scheme. The usual method of testing such a model by comparing its output to the evolution of a perturbation in a nonlinear model will indicate how well the linear model represents the behaviour of the discrete nonlinear model. This is expected from the theoretical analysis and has been illustrated with numerical experiments. However, if the limitations of the numerical scheme are not understood, the linear model will not necessarily indicate the true evolution of a perturbation in reality, for example a perturbation to the atmosphere, and so may not be valid for applications whic

the scheme to the continuous linear equation, for example by using the linearization state at a different time level, then the order of accuracy may be reduced. In practice we may want to make such approximations, since for example it may be too expensive to store the linearization state at every time step. It is clear from the simple example considered that any approximations made must take into account the effect on the truncation error. We next consider such questions in the context of a one-dimensional shallow-water model.

Chap er 5

A 1-D shallow wa er mo el

In the previous chapter we have shown that for a simple ordinary differential equation problem linearizing a discrete nonlinear model is not necessarily the same as discretizing the linearized continuous equations. We now examine this problem for a partial differential equation system, using some of the numerical schemes that are used in operational weather forecasting models. We begin in Section 5.1 by setting up the analytical model. We state the systems of nonlinear and linearized equations and examine some of their properties. In Section 5.2 we then present the various numerical schemes. We set out in detail the scheme for our nonlinear model and then discretize it to form the tangent linear model (TLM). We then present the result of applying a numerical scheme to the linearized equations, that is the perturbation forecast model (PFM). In dealing with partial differential equations we find that there is more freedom in how to apply the numerical scheme to the linearized equations and so two alternatives for the PFM are presented. Some analysis of the schemes is made in Section 5.3 before presenting the results from numerical experiments in Section 5.4. We then consider the effect of altering the time lev

chapter, particularly concentrating on those results which help our understanding of the three-dimensional models.

5.1 The analytical model

5.1.1 The nonlinear equations

The model we wish to consider is the one-dimensional shallow water system describing the flow of a single-layer fluid over an obstacle in the absence of rotation. The governing equations can be written

$$\frac{Du}{Dt} + \frac{\partial \phi}{\partial x} = -g\frac{\partial H}{\partial x}, \tag{5.1}$$

$$\frac{D\phi}{Dt} + \phi\frac{\partial u}{\partial x} = 0, \tag{5.2}$$

where

$$\frac{D}{Dt} = \frac{\partial}{\partial t} + u\frac{\partial}{\partial x} \tag{5.3}$$

is the material derivative. In these equations $H = H(x)$ is the height of the bottom orography, u is the velocity of the fluid and $\phi =$

When we implement the numerical model we find this form of the equation easier to work with, since the last term on the left hand side is linear. However, for work on the properties of the analytical equations, the two forms are equivalent and so we use (5.2).

5.1.2 Properties of the analytical system

from which we can derive the analytical dispersion relation

$$\omega = -kU_0 \pm k\sqrt{\Phi_0}. \tag{5.9}$$

The phase speed of a wave is then given by

$$-\frac{\omega}{k} = U_0 \pm \sqrt{\Phi_0}. \tag{5.10}$$

Thus for the linearized homogeneous analytical system the phase speed is independent of the wave number k.

For the complete nonlinear inhomogeneous system (5.1), (5.2), it is more difficult to obtain analytical properties. We can however find steady state solutions to the equations. To find such solutions we set $\partial u/\partial t = 0$ in (5.1) and

have

$$u(x,t) = \bar{u}(x,t) + \delta u(x,t), \tag{5.13}$$

$$\phi(x,t) = \bar{\phi}(x,t) + \delta\phi(x,t). \tag{5.14}$$

These expressions are substituted into the nonlinear equations (5.1), (5.2) and products of perturbations neglected, to give the linear equations. We obtain, for the linearization of the momentum equation (5.1)

$$\frac{D\delta u}{Dt} + \delta u \frac{\partial \bar{u}}{\partial x} + \frac{\partial \delta\phi}{\partial x}$$

5.2 The numerical schemes

5.2.1 The nonlinear model

The governing equations we discretize are the momentum equation (5.1) and the logarithmic form of the continuit

boundary conditions, such that the point ϕ_{N+1} is identical to the point ϕ_1 and $u_{N+\frac{1}{2}}$ is identical to $u_{\frac{1}{2}}$. Interpolation of quantities between u-points and ϕ-points is performed using a linear interpolation. The introduction of such a staggering means that for a general ϕ-point x_i and a general u-point $x_{i+\frac{1}{2}}$ the departure points will differ. Henceforth we indicate the departure point for the ϕ-point using the subscript $d\phi$ and the departure point for a u-poin

x_d can be calculated from

$$x_d = x_j - \alpha_j \tag{5.24}$$

where the displacement α_j is calculated using the iterative procedure introduced in Section 2.4,

$$\alpha_j^{(k+1)} = \Delta t u^*(x_j - \frac{\alpha_j^{(k)}}{2}, t_n + \frac{\Delta t}{2}) \tag{5.25}$$

with $\alpha_j^{(0)} = 0$. The velocity u^* is an estimate of the velocity at the mid-point of the trajectory. In order to estimate the velocity at time $t_n + \Delta t/2$ we use the extrapolation formulae

$$u^*(x_{i+\frac{1}{2}}, t_n + \frac{\Delta t}{2}) = \frac{3}{2}u(x_{i+\frac{1}{2}}, t_n) - \frac{1}{2}u(x_{i+\frac{1}{2}}, t_n - \Delta t) \tag{5.26}$$

at u points and

$$u^*(x_i, t_n + \frac{\Delta t}{2}) = \frac{3}{2}\overline{u}^x(x_i, t_n) - \frac{1}{2}\overline{u}^x(x_i, t_n - \Delta t) \tag{5.27}$$

at ϕ points, with

$$\overline{u}^x(x_i, t_n) = \frac{1}{2}(u(x_{i-\frac{1}{2}}, t_n) + u(x_{i+\frac{1}{2}}, t_n)). \tag{5.28}$$

The evaluation of (5.25) requires u to be calculated at the point $x_j - \alpha_j^{(k)}/2$. This may not lie on a grid poin

where INT(x) means the integer value of x. Now define $\gamma_j^{(k)}$ to be the fraction of the grid interval $x_{j-s} - x_{j-s-1}$ which is covered by the length $x_{j-s} - x_m$, so that

$$\gamma_j^{(k)} = -s_j^{(k)} + \frac{\alpha_j^{(k)}}{2\Delta x}. \tag{5.30}$$

Then u at point x_m can be calculated from the linear interpolation formula

$$\begin{aligned} u(m\Delta x, (n+\frac{1}{2})\Delta t) &= \gamma_j^{(k)} u((j - s_j^{(k)} - 1)\Delta x, (n+\frac{1}{2})\Delta t) \\ &+ (1 - \gamma_j^{(k)}) u((j - s_j^{(k)})\Delta x, (n+\frac{1}{2})\Delta t). \end{aligned} \tag{5.31}$$

Having performed K iterations of (5.25) the departure point is situated at $j\Delta x - \alpha_j^{(K)}$. It is normally found that there is no advantage to performing more than two iterations of this part of the solution procedure [79]. We now let

$$p = INT\left(\frac{\alpha_j^{(K)}}{\Delta x}\right. \tag{5.32}$$

and define

$$\beta_j = -p + \left(\frac{\alpha_j^{(K)}}{\Delta x}\right. \quad . \tag{5.33}$$

Then the departure point x_d lies between the points x_{j-p-1} and x_{j-p} and is a distance $\beta_j \Delta x$ from the point x_{j-p}, as shown in Figure 5.1. We note here that the INT function used in (5.29) and (5.32) is non-differentiable. Thus it will require special attention when we look at the tangent linear model.

2. Having found the departure points, we can calculate the right hand sides of (5.22) and (5.23). We first define the variables X, Y,

$$\begin{aligned} X &= u - (1-\alpha_1)\Delta t \left(\frac{\partial \phi}{\partial x} + g\frac{\partial H}{\partial x}\right), \\ Y &= \ln \phi - (1-\alpha_2)\Delta t \frac{\partial u}{\partial x}, \end{aligned} \tag{5.34}$$

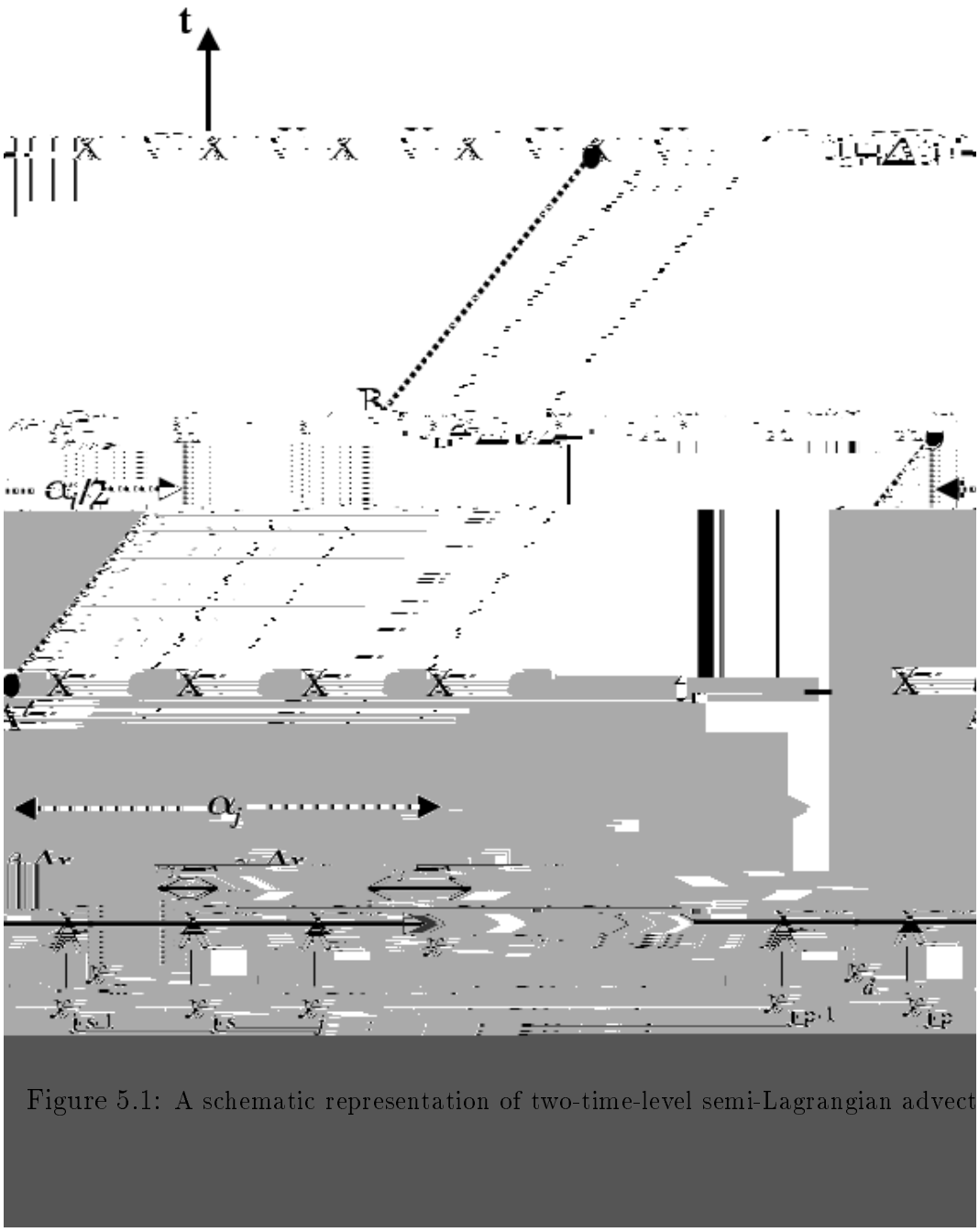

Figure 5.1: A schematic representation of two-time-level semi-Lagrangian advection.

$$\left.\frac{\partial u}{\partial x}\right|_i \approx \frac{u_{i+\frac{1}{2}} - u_{i-\frac{1}{2}}}{\Delta x}. \tag{5.37}$$

quations (5.22) and (5.23) thus become

$$u_{i+\frac{1}{2}}^{n+1} + \alpha_1 \Delta t \left(\left.\frac{\partial \phi}{\partial x}\right|_{i+\frac{1}{2}}^{n+1} + g \left.\frac{\partial H}{\partial x}\right|_{i+\frac{1}{2}} \right) = X_{du}^n, \tag{5.38}$$

$$(\ln \phi)_i^{n+1} + \alpha_2 \Delta t \left.\frac{\partial u}{\partial x}\right|_i^{n+1} = Y_{d\phi}^n. \tag{5.39}$$

The variables X and Y are calculated at gridpoints at time level n, defining X on u-points and Y on ϕ-points. The values at the departure points can then

$$u^{n+1}_{i+\frac{1}{2}} + \alpha_1 \Delta t \left(\left.\frac{\partial \phi}{\partial x}\right|^{n+1}_{i+\frac{1}{2}} + g \left.\frac{\partial H}{\partial x}\right|_{i+\frac{1}{2}} \right) = X^n_{du}, \tag{5.42}$$

$$(\ln \phi)^{n+1}_i + \alpha_2 \Delta t \left.\frac{\partial u}{\partial x}\right|^{n+1}_i = Y^n_{d\phi}, \tag{5.43}$$

valid for all values $i = 1, \ldots, N$, with periodic boundary conditions closing the system. Then eliminating $u_{i+\frac{1}{2}}$ for all values of i we obtain the set of equations

$$-\frac{\alpha_1 \alpha_2 \Delta t^2}{\Delta x^2}\phi^{n+1}_{i+1} + 2\frac{\alpha_1 \alpha_2 \Delta t^2}{\Delta x^2}\phi^{n+1}_i - \frac{\alpha_1 \alpha_2 \Delta t^2}{\Delta x^2}\phi^{n+1}_{i-1} + (\ln \phi)^{n+1}_i = R_i, \tag{5.44}$$

with

$$R_i = Y^n_{d\phi} - \frac{\alpha_2 \Delta t}{\Delta x}[\tilde{X}^n_{i+\frac{1}{2}} - \tilde{X}^n_{i-\frac{1}{2}}] \tag{5.45}$$

and

$$\tilde{X}^n_{i+\frac{1}{2}} = X^n_{du} - \alpha_1 \Delta t g \left.\frac{\partial H}{\partial x}\right|_{i+\frac{1}{2}}. \tag{5.46}$$

The equation (5.44) is a discretization of an elliptic equation on the domain and is weakly nonlinear through the presence of the $\ln \phi$ term on the left hand side.

4. A suitable procedure must now be obtained to solve the system (5.44) for all values of ϕ_i at time level $n + 1$. The method we choose is to apply a fixed point iteration, solving a linear problem on each iteration. A natural way of choosing such an iteration would be to consider a sc

$$\mathrm{I} \quad \alpha \quad \alpha_\phi \, \Delta D_D$$

and put

$$C = \frac{\alpha_1 \alpha_2 \Delta t^2}{\Delta x^2}. \tag{5.49}$$

Then substituting into (5.44) and moving the nonlinear term to the right hand side we have

$$-C\phi'_{i+1} + 2C\phi'_i - C\phi'_{i-1} = R_i - \ln(\Phi_{teuixwuxuuiuutuuuRuitwsdux/-/ \atop iutuuuuutuuwuuu} C\phi$$

5. As a final step we use these new values of ϕ_i to calculate values of u at each grid point at the new time level from (5.38), thus completing one time step of the scheme.

5.2.2 The tangent linear model

The normal procedure to obtain a tangent linear model is to linearize directly the source code of the nonlinear model, and this is the practice which we alsoand[fffffPoFPtheF

$$\begin{aligned}
\alpha_j^{(k+1)} &= \Delta t \Bigg[\frac{3}{2} \Big(\gamma_j^{(k)} u((j - s_j^{(k)} - 1)\Delta x, n\Delta t) \\
&\quad + (1 - \gamma_j^{(k)}) u((j - s_j^{(k)})\Delta x, n\Delta t) \Big) \\
&- \frac{1}{2} \Big(\gamma_j^{(k)} u((j - s_j^{(k)} - 1)\Delta x, (n-1)\Delta t) \\
&\quad + (1 - \gamma_j^{(k)}) u((j - s_j^{(k)})\Delta x, (n-1)\Delta t) \Big) \Bigg]. \qquad (5.58)
\end{aligned}$$

The equations resulting from a direct linearization of this discrete scheme are therefore as follows.

$$\delta s_j^{(k)} = 0,$$

with $\delta\alpha_j^{(0)} = 0$. We note here that because we are taking a small predetermined number of iterations, usually two or three, we can consider this as just a two- or three-step calculation and so linearize each iteration separately as if they were just different parts of the numerical scheme. This allows the linearization to be performed at the level of the model source code and is the procedure often followed in deriving the linearization of this part of a semi-Lagrangian scheme in meteorological models [64], [82]. However, when w

Lagrange interpolation to the departure points. Thus from (5.40) we have

$$
\begin{aligned}
\delta X^n_{du} &= (-\frac{1}{6}\beta_{i+\frac{1}{2}} + \frac{1}{6}\beta^3_{i+\frac{1}{2}})\delta X^n_{i+\frac{1}{2}-p-2} + (\beta_{i+\frac{1}{2}} + \frac{1}{2}\beta^2_{i+\frac{1}{2}} - \frac{1}{2}\beta^3_{i+\frac{1}{2}})\delta X^n_{i+\frac{1}{2}-p-1} \\
&+ (1 - \frac{1}{2}\beta_{i+\frac{1}{2}} - \beta^2_{i+\frac{1}{2}} + \frac{1}{2}\beta^3_{i+\frac{1}{2}})\delta X^n_{i+\frac{1}{2}-p} \\
&+ (-\frac{1}{3}\beta_{i+\frac{1}{2}} + \frac{1}{2}\beta^2_{i+\frac{1}{2}} - \frac{1}{6}\beta^3_{i+\frac{1}{2}})\delta X^n_{i+\frac{1}{2}-p+1} \\
&+ (-\frac{1}{6} + \frac{1}{2}\beta^2_{i+\frac{1}{2}})\delta\beta_{i+\frac{1}{2}}\bar{X}^n_{i+\frac{1}{2}-p-2} + (1 + \beta_{i+\frac{1}{2}} - \frac{3}{2}\beta^2_{i+\frac{1}{2}})\delta\beta_{i+\frac{1}{2}}\bar{X}^n_{i+\frac{1}{2}-p-1} \\
&+ (-\frac{1}{2} - 2\beta_{i+\frac{1}{2}} + \frac{3}{2}\beta^2_{i+\frac{1}{2}})\delta\beta_{i+\frac{1}{2}}\bar{X}^n_{i+\frac{1}{2}-p} \\
&+ (-\frac{1}{3} + \beta_{i+^1}
\end{aligned}
$$

turbation of X evaluated at the point X_{du} and similarly for $\delta Y^n_{d\phi}$. We define

(δX)

We note that the first term of each bracket on the right hand sides of (5.73) and (5.74) also appear in the analytical linear equations (5.15) and (5.17). However the second term of each bracket consisting of second derivatives of the linearization state do not appear in the analytical equations and thus do not appear in the perturbation forecast models. These terms arise from the perturbation to the departure point calculation. We see later in Section 5.3.3 that these terms contribute to the first order part of the truncation error for this scheme.

3. The next part of the nonlinear scheme is the iterative solution of the discrete elliptic equation. In order to find the tangent linear model we do not linearize this iterative procedure, but instead linearize the discrete equation of the nonlinear model and then solve this linear equation, thus following the normal procedure of automatic differentiation [5]. The equation which we solve in the nonlinear model is (5.51), but since this is mathematically equivalent to the original form (5.44), a linearization of the latter is sufficient. Linearizing (5.44) we obtain

$$-C\delta\phi_{i+1}^{n+1} + \left(2C + \frac{1}{\bar{\phi}_i^{n+1}}\right)\delta\phi_i^{n+1} - C\delta\phi_{i-1}^{n+1} = \delta R_i, \tag{5.75}$$

with C defined by (5.49) and

$$\delta R_i = \delta Y_{d\phi}^n - \frac{\alpha_2 \Delta t}{\Delta x}[\delta\tilde{X}_{i+\frac{1}{2}}^n - \delta\tilde{X}_{i-\frac{1}{2}}^n]. \tag{5.76}$$

This is a linear equation which can be solved directly for $\delta\phi_i^{n+1}$ at all points x_i. Hence we see that for this system an iterative procedure is not needed in the tangent linear model.

4. From the updated values of $\delta\phi_i$, the time level $n+1$ values of $\delta u_{i+\frac{1}{2}}$ at each point $x_{i+\frac{1}{2}}$ are then found from the linearization of (5.38)

$$\delta u_{i+\frac{1}{2}}^{n+1} = \delta\tilde{X}_{i+\frac{1}{2}}^n - \alpha_1 \Delta t \frac{(\delta\phi_{i+1}^{n+1} - \delta\phi_i^{n+1})}{\Delta x}. \tag{5.77}$$

This completes one time step of the tangent linear model.

5.2.3 The perturbation forecast model

To dev

1. We first calculate the departure points. Since the semi-Lagrangian part of our scheme is only considering advection by the linearization state wind, these departure points and hence their derivation is exactly the same as in the nonlinear model.

2. The next step is to calculate all the time level n terms in (5.78) and (5.79). We first define

$$\delta X = \delta u - (1-\alpha_1)\Delta t \underline{\frac{\partial \delta \phi}{}}$$

We can eliminate δu provided that

$$1 + \alpha_3 \Delta t \frac{\partial \bar{u}}{\partial x}\bigg|_{i+\frac{1}{2}}^{n+1} \neq 0. \tag{5.88}$$

This leads to a restriction on the time step

$$\Delta t < \frac{1}{\alpha_3 |\partial \bar{u}/\partial x|}, \tag{5.89}$$

This may seem to be an extra restriction which is not present in the tangent linear model. However, we recall from Section 2.4 that the iterative procedure by which we calculate the departure point itself imposes the restriction $\Delta t \max |\partial \bar{u}/\partial x| < 1$. Hence for values of α_3 in the range $[0, 1]$, (5.89) must hold in any case. We define

$$\bar{Z}_{i+\frac{1}{2}} = \left(1 + \alpha_3 \Delta t \frac{(\bar{u}_{j+\frac{3}{2}} - \bar{u}_{j-\frac{1}{2}})}{2\Delta x}\right)^{-1}, \tag{5.90}$$

so that (5.87) gives

$$\delta u_{i+\frac{1}{2}}^{n+1} = \bar{Z}_{i+\frac{1}{2}}^{n+1} \left(\delta X_{du}^n - \alpha_1 \Delta t \left. \frac{\partial \delta \phi}{\partial x} \right|_{i+\frac{1}{2}}^{n+1} \right. . \tag{5.91}$$

Then substituting this expression into (5.86) and rearranging, we obtain the system of linear equations

$$\begin{aligned} - \quad & C_{2i+\frac{1}{2}}(C_{1i} + C_3)\delta\phi_{i+1}^{n+1} \\ + \quad & \left[\frac{1}{\phi_i^{n+1}} + C_{2i-\frac{1}{2}}(-C_{1i} + C_3) + C_{2i+\frac{1}{2}}(C_{1i} + C_3)\right]\delta\phi_i^{n+1} \\ + \quad & C_{2i-\frac{1}{2}}(C_{1i} - C_3)\delta\phi_{i-1}^{n+1} \\ & = \delta R_i, \end{aligned} \tag{5.92}$$

with

$$
\begin{aligned}
C_{1i} &= \frac{\alpha_4 \Delta t}{2} \frac{\partial (\ln \bar{\phi})_i^{n+1}}{\partial x}, \\
C_{2_{i+\frac{1}{2}}} &= \frac{\alpha_1 \Delta t}{\Delta x} \bar{Z}_{i+\frac{1}{2}}^{n+1}, \\
C_3 &= \frac{\alpha_2 \Delta t}{\Delta x}, \\
\delta R_i &= \delta Y_j - C_{1j} (\bar{Z}_{j-\frac{1}{2}}^{n+1} \delta X_{j-\frac{1}{2}}^n + \bar{Z}_{j+\frac{1}{2}}^{n+1} \delta X_{j+\frac{1}{2}}^n) \\
&\quad - C_3 (\bar{Z}_{j+\frac{1}{2}}^{n+1} \delta X_{j+\frac{1}{2}}^n - \bar{Z}_{j-\frac{1}{2}}^{n+1} \delta X_{j-\frac{1}{2}}^n).
\end{aligned}
$$

The system (5.92) is represented by a strictly diagonally dominant tridiagonal matrix and so can be directly solved for all values of $\delta \phi_i^{n+1}$ using the same solver as in the nonlinear model.

4. The result of the previous step is then substituted into (5.91) to calculate the updated values $\delta u_{i+\frac{1}{2}}^{n+1}$ and so complete one time step of the perturbation forecast model.

5.2.4 A second v

the perturbation wind is likely to be small, we treat this term explicitly and in an ulerian fashion. Hence for both equations the term is evaluated at the arrival point, but at time level n. Thus we have the scheme

$$\begin{aligned}\frac{1}{\Delta t}\left(\delta u^{n+1}_{i+\frac{1}{2}} - \delta u^{n}_{du}\right) &+ \left(\delta u \frac{\partial \bar{u}}{\partial x}\right)^{n}_{i+\frac{1}{2}} \\ &+ (1-\alpha_1)\frac{\partial \delta\phi}{\partial x}\bigg|^{n}_{du} + \alpha_1 \frac{\partial \delta\phi}{\partial x}\bigg|^{n+1}_{i+\frac{1}{2}} = 0, \end{aligned} \tag{5.94}$$

$$\begin{aligned}\frac{1}{\Delta t}\left(\left(\frac{\delta\phi}{\bar{\phi}}\right)^{n+1}_{i} - \left(\frac{\delta\phi}{\bar{\phi}}\right)^{n}_{d\phi}\right. &+ \left(\overline{\delta u}^{x} \frac{\partial(\ln\bar{\phi})}{\partial x}\right)^{n}_{i} \\ &+ (1-\alpha_2)\frac{\partial \delta u}{\partial x}\bigg|^{n}_{d\phi} + \alpha_2 \frac{\partial \delta u}{\partial x}\bigg|^{n+1}_{i} = 0, \end{aligned} \tag{5.95}$$

with $\overline{\delta u}^{x}$ defined by (5.80). The method for solving this scheme is very similar to the previous section, with just a few terms changed. The departure point calculation is the same, from which we calculate the known terms

$$\delta X^{n}_{du} = \left(\delta u - (1-\alpha_1)\Delta t \frac{\partial \delta\phi}{\partial x}\right)^{n}_{du} - \Delta t \delta u \frac{\partial \bar{u}}{\partial x}\bigg|^{n}_{i+\frac{1}{2}}, \tag{5.96}$$

$$\delta Y^{n}_{d\phi} = \left(\frac{\delta\phi}{\bar{\phi}} - (1-\alpha_2)\Delta t \frac{\partial \delta u}{\partial x}\right)^{n}_{d\phi} - \Delta t \overline{}$$

Again we have a strictly diagonally dominant system, which can be solved for $\delta\phi_i$ at each point x_i for time level $n+1$. The result is then used to update $\delta u_{i+\frac{1}{2}}$ for all values of i by means of (5.98).

5.3

$$\frac{\delta\phi_i^{n+1} - \delta\phi_{d\phi}^n}{\Phi_0 \Delta t} + (1-\alpha_2)\left.\frac{\partial \delta u}{\partial x}\right|_{d\phi}^{n} + \alpha_2 \left.\frac{\partial \delta u}{\partial x}\right|_{i}^{n+1} = 0, \tag{5.103}$$

where $x_{du} = x_{i+\frac{1}{2}} - U_0 \Delta t$, $x_{d\phi} = x_i - U_0 \Delta t$ and the spatial derivatives are approxi-

Since $|E| = |E'|$, the condition $|E$

described in Section 5.2.1 we find that the semi-discrete scheme (5.20) satisfies the analytical momentum equation (5.1) with truncation error

$$\tau_u^{NL} = (2\alpha_1 - 1)\frac{\Delta t}{2}(\phi_{xt} + u\phi_{xx} + ugH_{xx})_{x_m}^{t_m} + O(\Delta t^2) \tag{5.114}$$

and that the scheme (5.21) satisfies the analytical continuity equation (5.4) with truncation error

$$\tau_\phi^{NL} = (2\alpha_2 - 1)\frac{\Delta t}{2}(u_{xt} + uu_{xx})_{x_m}^{t_m} + O(\Delta t^2). \tag{5.115}$$

We see that if we have $\alpha_1 = 0.5, \alpha_2 = 0.5$ then the scheme is second order accurate, whereas for the off-centred scheme, with α_1, α_2 greater than 0.5, there is a first order time truncation error. However, if the values are chosen to be close to 0.5, then we can write $\alpha_i = (1 + \epsilon_i)/2$, with $i = 1, 2$, for some small parameters ϵ_i. In this case we have for both equations

$$\tau^{kt}$$

the departure point, and then dropping products of perturbations in the expansion of the truncation error. We find that the tangent linear model satisfies the linearized momentum equation (5.15) with truncation error

$$\tau_u^{TL} = (2\alpha_1 - 1)\frac{\Delta t}{2}\left[\delta\phi_{xt} + \bar{u}\delta\phi_{xx} + \delta u\bar{\phi}_{xx} + \delta u g H_{xx}\right]_{x_m}^{t_m} + O(\Delta t^2) \qquad (5.117)$$

and the linearized continuity equation (5.17) with truncation error

$$\tau_\phi^{TL}(2\alpha_2 - 1)\frac{\Delta t}{2}\left[\delta u_{xt} + \bar{u}\delta u_{xx} + \delta u\bar{u}_{xx}\right]_{x_m}^{t_m} + O(\Delta t^2)$$

analytical linear equation (5.17) with truncation error

$$\begin{aligned}\tau_{\phi}^{P1} &= (2\alpha_2 - 1)\frac{\Delta t}{2}\left(\delta u_{xt} + \bar{u}\delta u_{xx}\right)_{x_m}^{t_m} \\ &+ (2\alpha_4 - 1)\frac{\Delta t}{2}((\delta u(\ln\bar{\phi})_x)_t + \bar{u}(\delta u(\ln\bar{\phi})_x)_x)_{x_m}^{t_m} + O(\Delta t^2). \quad (5.120)\end{aligned}$$

It is informative to compare the truncation errors of the tangent linear model and the first perturbation forecast model for our shallow water system. We consider first the approximation to the linearized momentum equation. A comparison of (5.117) and (5.119) shows that if $\delta u = 0$ so that there is no perturbation to the back trajectory of the semi-Lagrangian scheme, then the truncation errors are identical. Where $\delta u \neq 0$ an extra $O(\Delta t)$ error is added depending on how the perturbation to

error

$$\begin{aligned} \tau_u^{P2} &= (2\alpha_1 - 1)\frac{\Delta t}{2}\left(\delta\phi_{xt} + \bar{u}\delta\phi_{xx}\right)_{x_m}^{t_m} \\ &+ \frac{\Delta t}{2}\left(-(\delta u\bar{u}_x)_t + \bar{u}(\delta u\bar{u}_x)_x\right) + O(\Delta t^2) \end{aligned} \tag{5.121}$$

in the approximation of the linearized momentum equation (5.15) and the truncation error

$$\begin{aligned} \tau_\phi^{P2} &= (2\alpha_2 - 1)\frac{\Delta t}{2}(\delta u_{xt} + \bar{u}\delta u_{xx})_{x_m}^{t_m} \\ &+ \frac{\Delta t}{2}(-(\delta u(\ln\bar{\phi})_x)_t + \bar{u}(\delta u(\ln\bar{\phi})_x)_x) + O(\Delta t^2) \end{aligned} \tag{5.122}$$

in the approximation of (5.17). Thus we see that for this second version of the perturbation forecast model the accuracy is only first order in time even with the time weightings α_i set equal to 0.5. This appears to be a serious deficiency with this version of the model.

5.4 Numerical experiments

5.4.1 Verification of nonlinear model

The numerical experiment we use to test the different models is one of a motion forced by some orography, based on an experiment described by Houghton and Kasahara [38]. For time $t < 0$ the fluid is at rest and the geopotential ϕ is equal to $\phi_0 - H(x)$, with ϕ_0 constant. At $t = 0$ the fluid is impulsively set in motion with a constant velocity u_0 for all x. From this impulse a wave motion develops and moves away from the obstacle in both directions, while the solution in the vicinity of the obstacle becomes a steady state solution and thus satisfies (5.11) and (5.12). For a continuous flow the analytical values of the steady state constants K_1 and K_2 are

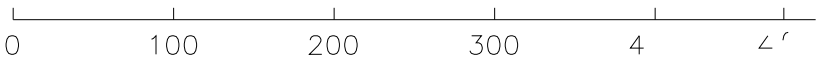
0
100
200
300
4

5.4.2 Verification of linear models

Before comparing the behaviour of the various linear models, we need to ensure that they are coded correctly. To do this we make use of the method described in Section 3.1 and compare the evolution of a perturbation in runs of each linear model with the difference between two runs of the nonlinear model. We take the experiment of Section 5.4.1 as our unperturbed run and add perturbations $(\gamma\delta u_0, \gamma\delta\phi_0)$ to the initial conditions in order to generate the perturbed runs. The initial perturbations are taken at $t = 0$ to be

$$\begin{aligned} \delta u_0 &= 0.01 m s^{-1}, \\ \delta\phi_0 &= -0.2 m^2 s^{-2}, \end{aligned}$$

Relative error for u field

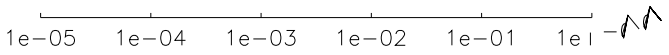

of a perturbation forecast model cannot be proved as easily as that of a tangent linear model. The analysis of Section 3.1.2 and the experimental evidence from these experiments show that the relative error will tend to a non-zero constant. However, it is not possible to tell from the value of that constant the significance of the difference between the perturbation forecast model and a tangent linear model. In Section 5.6 we test how well the method for testing a perturbation forecast model which we proposed in Section 3.3 can be used to assess this difference. First however we examine further the performance of the linear models with various numerical experiments.

5.4.3 Experiments with linear models

To begin we take the experiment of Section 5.4.1 as our nonlinear model run to produce the basic state, but we now use a time step of $\Delta t = 9.2 \times 10^{-3} s$. This is double the step we used previously, but we have found that the scheme remains stable with no noticeable loss in accuracy compared to runs with the smaller time step. The initial perturbation is taken to be

$$\begin{aligned} \delta u_0 &= 0.01 m s^{-1}, \\ \delta \phi_0 &= -0.2 m^2 s^{-2}. \end{aligned}$$

For each of the linear models we compare the perturbation produced by the linear model with the difference betweoeoeunmpare tPeoF6+l6+flflflPdu.oH+Φ0y=flflflPti+H5f

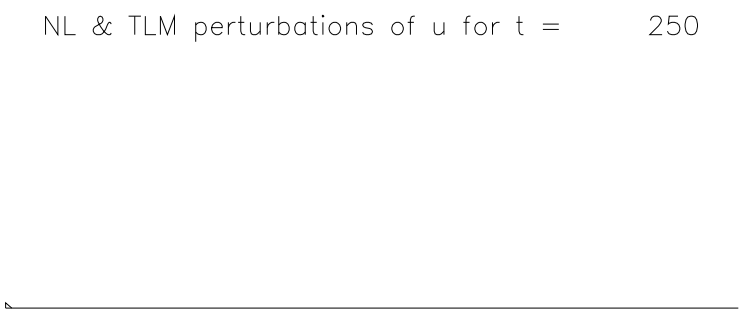
NL & TLM perturbations of u for t = 250

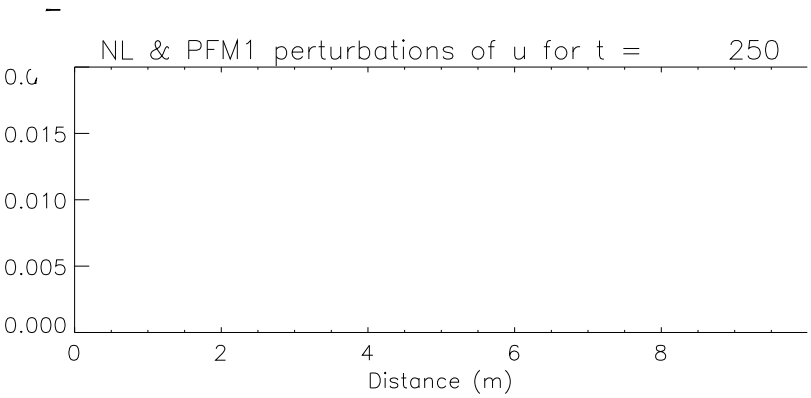
NL & PFM1 perturbations of u for t = 250
0.020
0.015
0.010
0.005
0.000
0
2
4
6
8
Distance (m)

NL

The first thing we notice from these pictures is that all the linear models seem to behave in the same way. For each of the models we see two main errors in the representation of the nonlinear perturbation. The first is that there is an amplitude error in the stationary solution in the centre of the domain. The second error is a phase error in the outwardly moving gravity waves. We examine the source of each of these in turn.

In order to understand the amplitude errors in the stationary solution, we refer back to the solutions derived in Section 5.1.2. There we found that that the stationary solution of the nonlinear model satisfies

$$u(x)\phi(x) = K_2 \tag{5.126}$$

and for this problem we have $K_2 = u_0\phi_0$. From this we can define a relationship between the perturbed quantities

$$\begin{aligned} E_N(x) &\equiv (\bar{u}(x) + \delta u(x))(\bar{\phi}(x) + \delta\phi(x)) - \bar{u}(x)\bar{\phi}(x) \\ &= \bar{u}(x)\delta\phi(x) + \delta u(x)\bar{\phi}(x) + \delta u(x)\delta\phi(x). \end{aligned} \tag{5.127}$$

Then using the asymptotic solutions we find that for the nonlinear problem the analytical value of $E_N(x)$ asymptotes to a constant value E_N^A, given by

$$E_N^A = u_0\delta\phi_0 + \delta u_0\phi_0 + \delta u_0\delta\phi_0. \tag{5.128}$$

We can define a similar quantity for the perturbations from the linear models. In Section 5.1.3 we found that the perturbation to the stationary solution satisfies two analytical expressions, given by (5.18) and (5.19). For the problem being described in this section we find that the constants $\delta K_1, \delta K_2$ are given by

$$\delta K_1 = u_0\delta u_0 + \delta\phi_0, \tag{5.129}$$

$$\delta K_2 = u_0\delta\phi_0 + \qquad\qquad t\ H$$

we find that for perturbations calculated from the linear problem $E_L(x)$ asymptotes to a constant value E_L^A given by

$$E_L^A = u_0 \delta\phi_0 + \delta u_0 \phi_0. \tag{5.132}$$

For the initial values used in the experiment of this section we find that $E_N^A = -0.02$ and $E_L^A = 0$.

For the numerical solutions we calculate E_N and E_L at the centre of the domain. We first interpolate u and δu to ϕ-points and then calculate the average value of $\bar{E_N}$ and $\bar{E_L}$ over an interval $[x_a, x_b]$ using the trapezoidal quadrature rule, which gives

$$\begin{aligned} \bar{E_N} &= \frac{1}{(x_b - x_a)} \left(\frac{1}{2} E_N(x_a) + \sum_{i=a+1}^{b-1} E_N(x_i) + \frac{1}{2} E_N(x_b) \right) , \\ \bar{E_L} &= \frac{1}{(x_b - x_a)} \left(\frac{1}{2} E_L(x_a) + \sum_{i=a+1}^{b-1} E_L(x_i) + \frac{1}{2} E_L(x_b) \right) . \end{aligned} \tag{5.133}$$

In Figure 5.9 we plot the variation over time of $\bar{E_N}$ calculated from the nonlinear perturbation and $\bar{E_L}$ calculated from the tangent linear model over the interval $x \in [4$. q

by the perturbation to u or the perturbation to ϕ. We therefore run again the previous experiment setting each of the initial perturbations to zero in turn. Thus for the first experiment we use

$$\delta u_0 = 0.01 m s^{-1}, \quad \delta \phi_0 = 0 m^2 s^{-2},$$

NL & TLM perturbations of u for t = 25

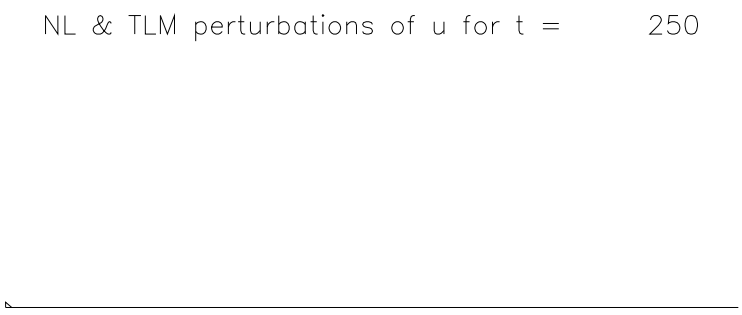
NL & TLM perturbations of u for t = 250

For each of these last two cases we still find an amplitude error in the centre of the domain. The reason for this is that when one of the perturbations is zero, then the asymptotic values E_N^A and E_L^A are equal. In the nonlinear model the nonlinear perturbation to $u\phi$ asymptotes to this expected value. In the linear model it is the linear perturbation to $u\phi$ which asymptotes to this quantity, and so an error is present according to the asymptotic value of the nonlinear term $\delta u(x)\delta\phi(x)$ calculated from the linear model. For the above experiment this quantity remains small for the case in which $\delta\phi_0$ is zero, which is why the amplitude error is less noticeable in Figure 5.10.

hnnVVa

solution. The initial conditions are

$$\begin{aligned} u(x,0) &= 10ms^{-1}, \\ \phi(x,0) &= 1000m^2s^{-2} + 100\exp\left[-\left(\frac{x-x_0}{5000}\right)^2\right]m^2s^{-2}. \end{aligned}$$

Then the solution of the ϕ field is two gravity waves which move in opposite directions. This is illustrated by Figure 5.12 which shows the initial and final fields of ϕ from a nonlinear model run using a time step $\Delta t = 1$. The average velocity of the waves in the numerical solution, calculated from the distance moved by each wave in the integration period, is $-22.7ms^{-1}$ for the left-moving wave and $42.7ms^{-1}$ for the right-moving wave. These values verify well with the analytical values of $-21.6ms^{-1}$ and $41.6ms^{-1}$ calculated from the phase speed (5.10) of the constant-coefficient homogeneous system given by (5.5) and (5.6). However, the amplitude of the waves is damped, with an amplitude of $1042m^2s^{-2}$ compared with the analytical solution of $1050m^2s^{-2}$. This damping can be reduced by using a smaller time-weighting coefficient, but at the expense of introducing some trailing waves. For the purpose of comparing the linear models we prefer the solution to be as clean as possible, and so we choose to remain with the damped solution.

We now look at two experiments with the linear models. The above experiment is taken as the linearization state and we obtain the perturbed state by adding perturbations

$$\begin{aligned} \delta u(x,0) &= 3ms^{-1}, \\ \delta\phi(x,0) &= -10\exp\left[-\left(\frac{x-x_0}{5000}\right)^2\right]m^2s^{-2}. \end{aligned}$$

For the two experiments we run for a total of $10,000s$. The first experiment uses a time step of $250s$ and

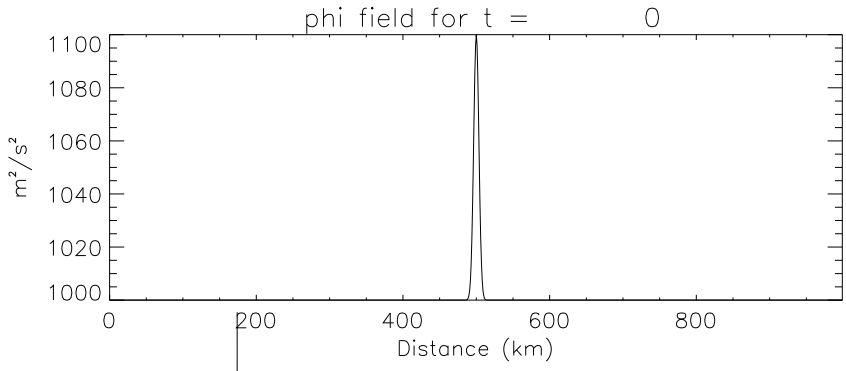
phi field for t = 0
1100
1080
1060
1040
1020
1000
m²/s²
0
200
400
600
800
Distance (km)

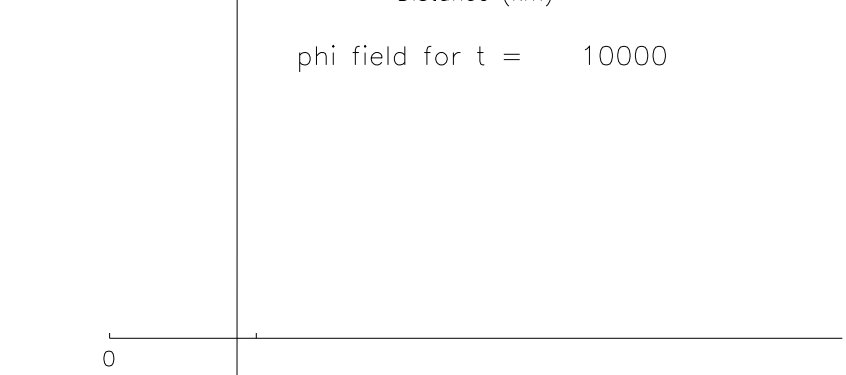
phi field for t = 10000
0

phi field for time step = 250

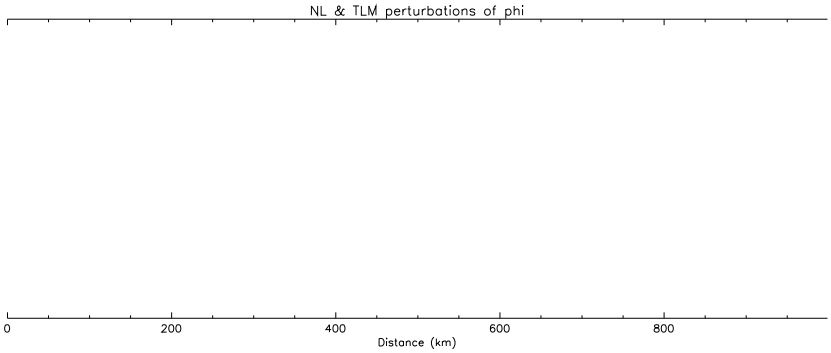
NL & TLM perturbations of phi
0
200
400
600
800
Distance (km)

problem of Chapter 4 this approximation still had the same second order accuracy as the original scheme. Thus for the first perturbation forecast model we replace (5.78) and (5.79) by

$$\begin{aligned}
& \frac{1}{\Delta t}\left(\delta u_{i+\frac{1}{2}}^{n+1} - \delta u_{du}^{n}\right) + (1-\alpha_1)\frac{\partial \delta\phi}{\partial x}\bigg|_{du}^{n} + \alpha_1 \frac{\partial \delta\phi}{\partial x}\bigg|_{i+\frac{1}{2}}^{n+1} \\
+ \quad & (1-\alpha_3)(\delta u)_{du}^{n}\left(\frac{\partial \bar{u}}{\partial x}\right)_{du}^{n+\frac{1}{2}} + \alpha_3(\delta u)_{i+\frac{1}{2}}^{n+1}\left(\frac{\partial \bar{u}}{\partial x}\right)_{i+\frac{1}{2}}^{n+\frac{1}{2}} = 0, \qquad (5.137) \\
& \frac{1}{\Delta t}\left(\frac{\delta\phi_i^{n+1}}{\bar{\phi}_i^{n+\frac{1}{2}}} - \frac{\delta\phi_{d\phi}^{n}}{\bar{\phi}_{d\phi}^{n+\frac{1}{2}}}\right) + (1-\alpha_2)\frac{\partial \delta u}{\partial x}\bigg|_{d\phi}^{n} + \alpha_2 \frac{\partial \delta u}{\partial x}\bigg|_{i}^{n+1} \\
+ \quad & (1-\alpha_4)\ \overline{\qquad}
\end{aligned}$$

An alternative method of approximating the linearization state at one time level only would be to average the time level n and time level $n+1$ values. However, since this averaging is an $O(\Delta t^2)$ approximation to the value at the middle of the time step, the zero order truncation error term appears in the same way.

We illustrate this error by repeating the first experiment of Section 5.4.3 for the first perturbation forecast model, which previously gave the result shown in Figure 5.7. We first rerun the experiment using a linearization state defined by the average of the time level n and time level $n+1$ values at the correct spatial point. The output at the end of the run is shown in Figure 5.16. It is clear that for both the u and ϕ fields the linear model solution is completely incorrect. If however we replace the linearization state in the $\delta\phi/\bar{\phi}$ terms of (5.138) with the correct values, but use the averaged values of the linearization state elsewhere in (5.137) and (5.138), then such a large error does not occur. The output from this experiment is shown in Figure 5.17, which is hard to distinguish from Figure 5.7.

It is possible to extend this analysis to show that a zero order term will occur with such an approximation to the linearization state wherever a time-varying linearization state is included within an advective term of the perturbation forecast model. In general this will be the case if the nonlinear model contains the semi-Lagrangian advection of a quantity which is a nonlinear function of the model variables. For example, in the nonlinear model of this chapter we advect $\ln\phi$ and so this leads to a $1/\bar{\phi}$ term in the perturbation forecast model advection. If we had chosen to discretize the alternative form of the mass continuity equation (5.2), which advects ϕ itself, then we would not have had a problem with consistency even with the time-averaged linearization state.

For the three-dimensional model being developed at the Met Office, which we discuss in Chapter 6, the problem of the zero-order term does not arise since all the quantities being advected are linear in the model variables. However, treating the logarithmic form of the continuity equation with a semi-Lagrangian scheme is

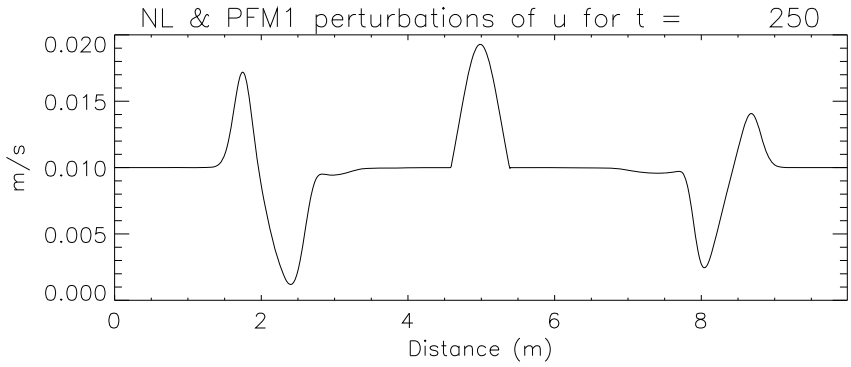
NL & PFM1 perturbations of u for t = 250
0.020
0.015
0.010
0.005
0.000
m/s
0
2
4
6
8
Distance (m)

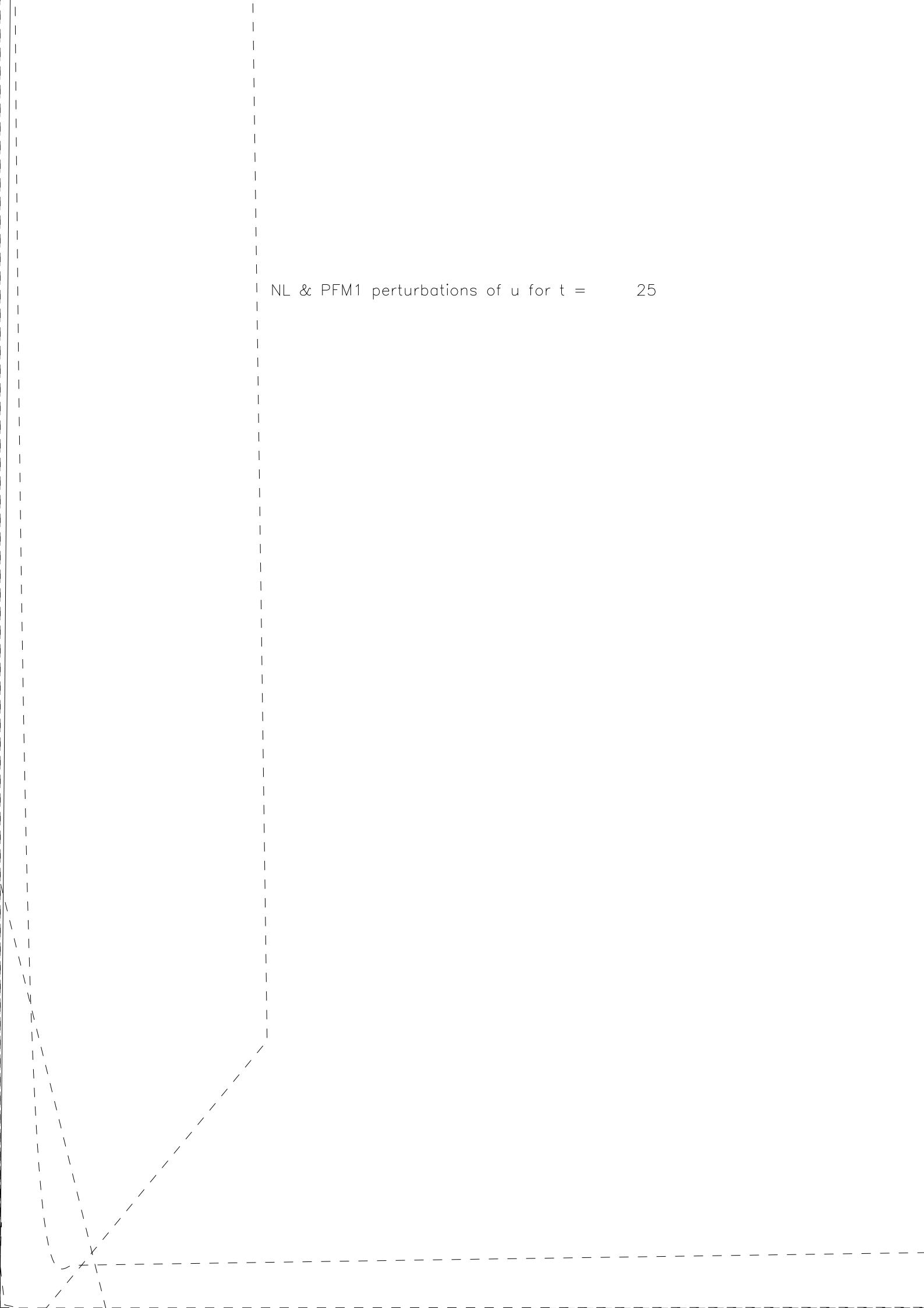
NL & PFM1 perturbations of u for t = 25

not uncommon. For example the operational models of the uropean Centre for Medium-range W

perturbations, the errors do not tend to zero as a perturbation becomes infinitesimally small. In the experiments so far in this chapter we have been able to verify the output of the perturbation forecast models by comparison with the tangent linear model. For the three-dimensional models being used at the Met Office we do not have this opportunity, since we only have the perturbation forecast model and do not have the tangent linear of the discrete nonlinear model. As a proposal for overcoming this problem we developed in Section 3.3 formulae for estimating the linearization error and solution error we would obtain if we were to use a tangent linear model. Since for the shallow water model of this chapter we have the true tangent linear available, we are able to verify the usefulness of these formulae.

In order to validate the formulae developed in Section 3.3 we run again the first experiment from Section 5.4.3. The nonlinear model is then run perturbed by a perturbation $(\gamma\delta u_0, \gamma\delta\phi_0)$, where we use values of $\gamma = 0.5$,

gamma = 0.5
0
50
100
150

using the estimate with $\gamma = 0.02$ introduces an error of approximately 1.5% in the calculation of the linearization error. Thus the estimate with this value of the parameter is also quantitatively very good. For the stationary solution in the centre of the domain the true linearization error is 1.3×10^{-3} and the estimate differs from this by approximately 0.25%. A further reduction in γ by a factor of 2 to 0.01 reduces the maximum difference by another factor of 2 to 3.4×10^{-5}. However, this is at the expense of introducing some noise due to rounding error, as can be seen from the third difference plot of Figure 5.20. Thus it seems that the values of $\gamma = 0.02$, which from the plots of solution error was conjectured to be the most suitable value of the parameter, does indeed provide a good compromise between accuracy of the formulae and rounding error.

The experiments of this section have shown that the formulae we derived in Section 3.3 can provide an accurate estimate of the linearization error and solution error of a tangent linear model using only the nonlinear model. This estimate is useful both qualitatively and quantitatively. Having demonstrated this numerically we can have some confidence in the use of these estimates in the three-dimensional model of Chapter 6, for which we do not have an exact tangent linear model. The numerical experiments have also provided a method of choosing the parameter γ such that we obtain a good balance between accuracy and the introduction of spurious noise.

5.7 Summary

In this chapter we have investigated the semi-continuous approach for producing a linear model in the context of a partial differential equation problem, using numerical schemes similar to those used in weather forecasting models. Beginning with a one-dimensional shallow water system we developed two versions of a perturbation forecast model and compared them to the tangent linear model derived by the

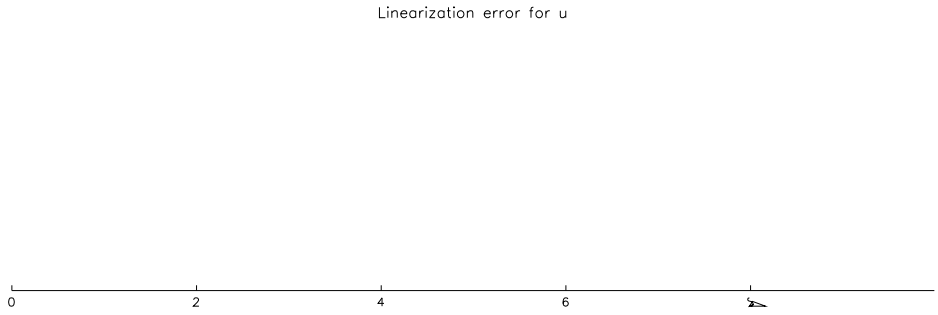
Linearization error for u
0
2
4
6

True error minus estimated error for u using gamma = 0.1

discrete approach. We have shown that the semi-continuous method can be used to design a linear model which is as equally valid as the tangent linear model for finite perturbations. However, this chapter has also illustrated several problems which can occur when using this approach and which must be taken into account when it is applied to a full weather forecasting model.

Firstly, it is clear that when we are treating a system of partial differential equations, there is some extra degree of freedom in deriving a perturbation forecast model which is not present in the ordinary differential equation problem. The linearization of the analytical equations can produce terms in the linear equations which have no obvious counterpart in the nonlinear model and so no obvious discretization. This was seen in the shallow water model of this chapter. The linearization of the analytical equations produced terms containing the perturbation wind multiplied by the gradient of the linearization state field. In the two versions of the perturbation forecast model described in Sections 5.2.3 and 5.2.4 we proposed two different ways of discretizing this term. Our analysis showed that one of these models was second order accurate in time for a centred time averaging, while the other remained first order for all choices of the time weightings. The tangent linear model was also second order for a centred time averaging. Thus we find that the development of a perturbation forecast model for a partial differential equation problem introduces the possibility of choosing a numerical scheme which is detrimental to the accuracy of the model. This illustrates the necessity of applying the semi-continuous method with great care and with a good understanding of the underlying numerical schemes.

We have also shown that the perturbation forecast model requires the time level of the linearization state to be chosen carefully. In the ordinary differential equation problem of Chapter 4 taking the linearization state at the centre of the time step was sufficient to retain second order accuracy, while using the linearization state at the start of the time step reduced the accuracy to first order. This was also true for the shallow water model of this chapter, provided that the correct linearization state

was used within the semi-Lagrangian advection scheme. However, if approximations were made to the linearization state within the advection scheme, then the resulting perturbation forecast model was no longer consistent. This reinforces the conclusion of Chapter 4 that any approximations in the linearization state must be considered in the context of the whole scheme.

Finally we have illustrated that a perturbation forecast model is more difficult to test than a tangent linear model since it is not correct in the sense of Definition 3.2 and so the relative error or solution error do not reduce to zero as the perturbation size is reduced. This provides a problem for testing our three-dimensional weather forecasting model, since we do not have the tangent linear model solution to compare with. To overcome this we developed in Chapter 3 a method of estimating the linearization error and solution error that a tangent linear model would have, by using only the nonlinear model. In this chapter we have been able to demonstrate that this method gives useful estimates and we have also introduced a practical method of specifying a value for the variable parameter γ which the method requires. Thus we can be more confident in the use of this estimate to assess the accuracy of our three-dimensional perturbation forecast model in Chapter 6.

Chap er 6

Applica ion o a Three-Dimensional Mo el

In Chapters 4 and 5 we have illustrated the viability of developing a linear model by the semi-continuous method. We now apply these ideas to a three-dimensional weather forecasting model. The model we use is the adiabatic version of the new integration scheme being developed at the Met Office for future operational use. The linearization of this model and the adjoint of the linear model are needed as part of the dev

to assess the validity of the model. These will be outlined as we discuss specific numerical results in Section 6.3.

6.1 The nonlinear model

6.1.1 The continuous equations

The nonlinear model is based on the fully compressible Navier-Stokes equations on a sphere. The equations are written in spherical coordinates (r, λ, ϕ), with a height based vertical coordinate, where r defines the distance from the centre of the earth. The horizontal coordinates λ, ϕ are the longitudinal and latitudinal directions on a regular latitude-longitude grid. The vertical levels in the numerical model are defined by a coordinate η, with the levels following the terrain near the surface of the model and gradually becoming flat higher in the atmosphere. We assume that the coordinate η is a smooth, differentiable function of r, with $\partial\eta/\partial r > 0$. The coordinate is defined such that $\eta = 0$ on the model level following the earth's surface and $\eta = 1$ on the top model level. Then derivatives along constant r surfaces can be written in terms of derivatives along constant η surfaces using the transformation

$$\left.\frac{\partial}{\partial s}\right|_r = \left.\frac{\partial}{\partial s}\right|_\eta - \left.\frac{\partial r}{\partial s}\right|_\eta \left.\frac{\partial}{\partial r}\right|_{\lambda,\phi,t}, \tag{6.1}$$

where $s = \lambda, \phi$ or t. This relationship also allows us to define a generalized vertical velocity $\dot{\eta}$ with respect to the coordinate system. Noting that the material derivative in height coordinates is given by

$$\frac{D}{Dt} \equiv \left.\frac{\partial}{\partial t}\right|_r + \frac{u}{r\cos\phi}\left.\frac{\partial}{\partial \lambda}\right|_r + \frac{v}{r}\left.\frac{\partial}{\partial \phi}\right|_r + w\frac{\partial}{\partial r} \tag{6.2}$$

we define a vertical velocity $\dot{\eta} = D\eta/Dt$. Then we find that $\dot{\eta}$ is related to w by means of the formula

$$\dot{\eta} = \frac{1}{\partial r/\partial \eta}\left[w - \frac{u}{r\cos\phi}\left.\frac{\partial r}{\partial \lambda}\right|_\eta - \frac{v}{r}\left.\frac{\partial r}{\partial \phi}\right|_\eta\right]. \tag{6.3}$$

The material derivative in the η coordinate system becomes

$$\frac{D}{Dt} \equiv \left.\frac{\partial}{\partial t}\right|_\eta + \frac{u}{r\cos\phi}\left.\frac{\partial}{\partial\lambda}\right|_\eta + \frac{v}{r}\left.\frac{\partial}{\partial\phi}\right|_\eta + \dot{\eta}\frac{\partial}{\partial\eta}. \tag{6.4}$$

The adiabatic form of the continuous model consists of the momentum equations in three dimensions, the mass continuity equation, the thermodynamic equation and the equation of state. These equations then take the following form in the model coordinates, where the notation is set out in Table 6.1, adapted from Table 1 of [18]:

$$\frac{Du}{Dt} - 2 \quad \sin\phi v + 2 \quad \cos\phi w - \frac{uvtan\phi}{r} + \frac{uw}{r} + \frac{c_p\theta}{rcos\phi}\left(\frac{\partial\Pi}{\partial\lambda} - \frac{\partial\Pi}{\partial r}\frac{\partial r}{\partial\lambda}\right) = 0, \tag{6.5}$$

$$\frac{Dv}{Dt} + 2 \quad \sin\phi u + \frac{u^2 tan\phi}{r} + \frac{vw}{r} + \frac{c_p\theta}{r}\left($$

(r, λ, ϕ)	Spherical polar coordinates relative to centre of arth
η	Terrain-following vertical coordinate
u, v, w	Velocity components
$\dot{\eta}$	Generalized vertical velocity
p, p_0	Pressure and reference value of pressure
Π	xner pressure $\left(\frac{p}{p_0}\right)^{\kappa}$
c_p	Specific heat of dry air at constant pressure
κ	Gas constant divided by c_p
ρ	Density scaled by r^2
θ	Potential temperature
	arth's rotation rate
f	2 $\sin\phi$ (Coriolis parameter)
g	Gravitational constant

Table 6.1: Symbols used in equations. Table adapted from Table 1 of [18].

6.1.2 The discrete nonlinear model

We present here a brief outline of the numerical scheme used in the nonlinear model. Fuller details of the implementation and justification for some of the choices made can be found in [18] and [19]. The model is implemented on a staggered grid, using an Arakawa C staggering in the horizontal and a Charney-Phillips staggering in the vertical. The scheme itself combines a semi-Lagrangian treatment of advection with a semi-implicit treatment of terms responsible for sound and gravity waves. The procedure used is a predictor-corrector method and consists of the following steps:

1. Predict initial estimates of updates to the wind components, density and potential temperature.

2. Use these predicted values and the equation of state to form an equation for the update to the pressure variable. [illegible]

Within the three-dimensional nonlinear model there are various predictor-corrector steps before the formation of the elliptic equation. This is to enable the nonlinear terms to be calculated as accurately as possible. However, if we were to linearize this discrete scheme we would require values of the linearization state from each predictor-corrector step either to be stored from the nonlinear model base state run or to be recalculated during each run of the linear model. We see in the scheme developed for the perturbation forecast model in Section 6.2 that by using the semi-continuous approach we avoid the need for these intermediate values.

Once the initial estimates of the corrections have been calculated, an elliptic equation for the pressure correction is formulated. In the nonlinear model this is done by first linearizing the equation of state (6.10). We define the time tendencies of ρ, θ and Π in one time step by

$$\rho' \equiv \rho^{n+1} - \rho^n, \qquad \theta' \equiv \theta^{n+1} - \theta^n, \qquad \Pi' \equiv \Pi^{n+1} - \Pi^n, \tag{6.11}$$

where n and $n+1$ indicate the time level. Then linearizing the equation of state in terms of these variables we obtain

$$\kappa \Pi \theta \rho' + \kappa \rho \theta \Pi' + \kappa \rho \Pi \theta' = -\kappa \rho \Pi \theta + \frac{r^2 p}{c_p}, \tag{6.12}$$

where the full model variables are defined at time level n. It is this equation which we solve within the numerical model. We substitute appropriate predicted quantities into (6.12) to obtain an elliptic equation for the pressure correction Π'. This step ensures that the elliptic equation obtained is linear, but at the expense of accuracy. An alternative strategy is to write the continuity equation in logarithmic form and retain the weakly nonlinear elliptic equation which results. This is the strategy adopted by the Canadian Meteorological Centre [16]. The presently used method leads to a linear Helmholtz equation, which is solved using a generalized conjugate

6.2 The perturbation forecast model

6.2.1 The continuous equations

We represent the state vector of the continuous nonlinear model by

$$\mathbf{x_c} = (u, v, w, \Pi, \rho, \theta). \tag{6.13}$$

The continuous equations for the perturbation forecast model are obtained by first setting

$$\mathbf{x_c} = \bar{\mathbf{x}}_\mathbf{c} + \boldsymbol{\delta}\mathbf{x_c}, \tag{6.14}$$

where $\bar{\mathbf{x}}_\mathbf{c}$ is a spatially and temporally varying background state satisfying the nonlinear equations and $\boldsymbol{\delta}\mathbf{x_c}$ is the perturbation vector

$$\boldsymbol{\delta}\mathbf{x_c} = (\delta u, \delta v, \delta w, \delta\Pi, \delta\rho, \delta\theta). \tag{6.15}$$

We then substitute into the nonlinear equations and drop products of perturbations in the usual way to obtain the linearized set of equations.

However, before carrying out this procedure we can use our physical insight to simplify the equation set that we wish to linearize. Firstly we omit in (6.5) and (6.6) the metric and Coriolis terms in which w appears and in the vertical velocity equation we omit the metric and Coriolis terms involving u and v. This is based on the commonly used "traditional approximation" [22]. However, whereas this approximation is usually preceded by assuming that $1/r$ may be replaced by $1/a$, where a is the constant radius of the arth (the shallow atmosphere approximation) [58], we retain a full three-dimensional height field in the equations. On the basis of a simple scale analysis we also make the extra approximation of ignoring the advection of w, treating the time derivative as a partial derivative. After all of these approximations the full set of momentum equations which we linearize is

$$\frac{Du}{Dt} - 2 \quad \sin\phi v - \frac{uvtan\phi}{r} +$$

$$\frac{Dv}{Dt} + 2 \quad \sin\phi u + \frac{u^2 tan\phi}{r} + \frac{c_p\theta}{r}\left(\frac{\partial\Pi}{\partial\phi} - \frac{\partial\Pi}{\partial r}\frac{\partial r}{\partial\phi}\right) = 0, \tag{6.17}$$

$$\frac{\partial w}{\partial t} + g + c_p\theta\frac{\partial\Pi}{\partial r} = 0. \tag{6.18}$$

Having made these approximations we perform the linearization procedure. For the linearization of the approximate momentum equations (6.16), (6.17) and (6.18) we obtain the linearized equations

$$\begin{aligned}\frac{D\delta u}{Dt} \quad & + \boldsymbol{\delta u}.\nabla\bar{u} - 2 \quad \sin\phi\delta v - \frac{\delta u\bar{v}\tan\phi}{r} - \frac{\bar{u}\delta v\tan\phi}{r} \\ & + \frac{c_p\delta\theta}{r\cos\phi}\left(\frac{\partial\bar{\Pi}}{\partial\lambda} - \frac{\partial\bar{\Pi}}{\partial r}\frac{\partial r}{\partial\lambda}\right) + \frac{c_p\bar{\theta}}{r\cos\phi}\left(\frac{\partial\delta\Pi}{\partial\lambda} - \frac{\partial\delta\Pi}{\partial r}\frac{\partial r}{\partial\lambda}\right) = 0,\end{aligned} \tag{6.19}$$

$$\begin{aligned}\frac{D\delta v}{Dt} \quad & + \boldsymbol{\delta u}.\nabla\bar{v} + 2 \quad \sin\phi\delta u + \frac{2\bar{u}\delta u\tan\phi}{r} \\ & + \frac{c_p\delta\theta}{r}\left(\frac{\partial\bar{\Pi}}{\partial\phi} - \frac{\partial\bar{\Pi}}{\partial r}\frac{\partial r}{\partial\phi}\right) + \frac{c_p\bar{\theta}}{r}\end{aligned}$$

right hand side of (6.12) is zero. Then ignoring products of perturbations with the time increments ρ', Π' and θ', we obtain the linearized equation

$$\kappa\bar{\Pi}\bar{\theta}(\delta\rho^{n+1} - \delta\rho^n) + (\kappa - 1)\bar{\rho}\bar{\theta}(\delta\Pi^{n+1} - \delta\Pi^n) + \kappa\bar{\Pi}\bar{\rho}(\delta\theta^{n+1} - \delta\theta^n) = 0. \qquad (6.24)$$

The six equations (6.19)-(6.24) form the basis of the perturbation forecast model. The symbol ∇ is the three-dimensional gradient operator, defined on a sphere as

$$\nabla = \left(\frac{1}{r\cos\phi}\frac{\partial}{\partial\lambda}, \mathrm{r}\right.$$

of the solution procedure more clearly. We first define a general state of the discrete perturbation forecast model

$$\boldsymbol{\delta}\mathbf{x} = (\delta u, \delta v, \delta w, \delta\Pi, \delta\rho, \delta\theta), \tag{6.28}$$

where the perturbation fields are now understood to be vectors of values over the model grid points. We let

$$\boldsymbol{\delta}\mathbf{x}' = \boldsymbol{\delta}\mathbf{x}^{n+1} - \boldsymbol{\delta}\mathbf{x}^{n}. \tag{6.29}$$

Then the scheme can be written in the simple form

$$\boldsymbol{\delta}\mathbf{x}^{n+1} = \boldsymbol{\delta}\mathbf{x}^{n} + \mathbf{M}^{-1}\mathbf{P}\boldsymbol{\delta}\mathbf{x}^{n}, \tag{6.30}$$

where $\mathbf{P}$ and $\mathbf{M}$ are matrices denoting the predictor and corrector parts of the scheme.

We note that the variable $\delta\dot{\eta}$ is not included within the vector $\boldsymbol{\delta}\mathbf{x}$, but is treated as a diagnostic quantity calculated at the start of each time step. The pressure variable is taken to be $\delta\Pi$, from which we can calculate δp using (6.26).

The first step of the solution procedure is to calculate the application of the matrix $\mathbf{P}$, which we denote

$$\boldsymbol{\delta}\tilde{\mathbf{x}} = \mathbf{P}\boldsymbol{\delta}\mathbf{x}^{n}. \tag{6.31}$$

This corresponds to the predictor step in the scheme. We must then invert the matrix $\mathbf{M}$ to complete the solution of (6.30). In practice we have the matrix in the operator form

$$\mathbf{M}\boldsymbol{\delta}\mathbf{x}' = \boldsymbol{\delta}\tilde{\mathbf{x}}. \tag{6.32}$$

This system is reduced analytically to a single equation for $\delta\Pi'$, of the form

$$\mathcal{L}\delta\Pi' = RHS, \tag{6.33}$$

where $\mathcal{L}$ is an elliptic operator, which can then be solved using a generalized conjugate residual (GCR) method. The value of $\delta\Pi'$ is then substituted into (6.32) to

follows a very similar semi-implicit semi-Lagrangian solution procedure. In this section we set out the semi-discretized form of the equations to indicate how the time discretization is implemented. A more complete description of the scheme is then given in Section 6.2.5. First it is necessary to introduce some notation for the representation of the finite difference equations.

Notation

We define finite difference operators for the horizontal and vertical grids. For the horizontal operators we let $X(\lambda_i, \phi_j)$ be a general point on the horizontal grid, where i, j are the indices in the λ and ϕ directions respectively and the vertical level is unspecified for the purpose of the definitions. For the vertical operators we consider a variable $Z = Z(r_{i,j,k})$ for operators involving r and $Z = Z(\eta_k)$ for operators involving η, where i, j represent the indices in the λ and ϕ directions and k is the vertical level. We then have

- Horizontal averaging operators

$$\begin{aligned} \overline{X(\lambda_i, \phi_j)}^{\lambda} &= \frac{1}{2}\left[X(\lambda_{i+\frac{1}{2}}, \phi_j) + X(\lambda_{i-\frac{1}{2}}, \phi_j)\right], \\ \overline{X(\lambda_i, \phi_j)}^{\phi} &= \frac{1}{2}\left[X(\lambda_i, \phi_{j+\frac{1}{2}}) + X(\lambda_i, \phi_{j-\frac{1}{2}})\right] \end{aligned} \tag{6.37}$$

- Vertical averaging operators

$$\overline{Z(r_{i,j,k})}^{r} = \frac{(r_{i,j,k+\frac{1}{2}} - r_{i,j,k})Z(r_{i,j,k+\frac{1}{2}}) + (r_{i,j,k} - r_{i,j,k-\frac{1}{2}})Z(r_{i,j,k-\frac{1}{2}})}{r_{i,j,k+\frac{1}{2}} - r_{i,j,k-\frac{1}{2}}}, \quad (6.43)$$

$$\overline{Z(\eta_k)}^{\eta} = \frac{(\eta_{k+\frac{1}{2}} - \eta_k)Z(\eta_{k+\frac{1}{2}}) + (\eta_k - \eta_{k-\frac{1}{2}})Z(\eta_{k-\frac{1}{2}})}{\eta_{k+\frac{1}{2}} - \eta_{k-\frac{1}{2}}}; \quad (6.44)$$

- Vertical differencing operators

$$\partial_r Z(r_{i,j,k}) = \frac{Z(r_{i,j,k+\frac{1}{2}}) - Z(r_{i,j,k-\frac{1}{2}})}{r_{i,j,k+\frac{1}{2}} - r_{i,j,k-\frac{1}{2}}}, \quad (6.45)$$

$$\partial_{2r} Z(r_{i,j,k}) = \frac{Z(r_{i,j,k+1}) - Z(r_{i,j,k-1})}{r_{i,j,k+1} - r_{i,j,k-1}}, \quad (6.46)$$

$$\partial_\eta Z(\eta_k) = \frac{Z(\eta_{k+\frac{1}{2}}) - Z(\eta_{k-\frac{1}{2}})}{\eta_{k+\frac{1}{2}} - \eta_{k-\frac{1}{2}}}, \quad (6.47)$$

$$\partial_{2\eta} Z(\eta_k) = Z(\eta_k$$

the parameter $\beta = f\Delta t$, where $f = 2 \sin\phi$ is the Coriolis parameter, and define weightings

$$W_1 = \frac{1 - \alpha_5(1-\alpha_5)\beta^2}{1 + \alpha_5^2\beta^2}, \tag{6.51}$$

$$W_2 = \frac{\beta}{1 + \alpha_5^2\beta^2}, \tag{6.52}$$

for a time-weighting parameter α_5.

respectively. We then have

$$\begin{aligned}\delta u^{n+1} &= W_1 \delta u^n_{du} - W_2 \delta v^n_{du} + \Delta t \Big[(\boldsymbol{\delta \mathbf{u}}.\nabla \bar{u})^n - \left(\frac{\delta u \bar{v} \tan\phi}{r} \right)^n \\ &+ \overline{\frac{c_p \delta\theta}{r \cos\phi} \Big(\partial}\end{aligned}$$

6.2.4 Comments on the discretization

It is useful at this point to highlight two particular differences from the scheme used in the nonlinear model. The first arises from the linearization of the advection terms which, as we discussed in Chapter 5, which produces an extra term consisting

where

$$\frac{D}{Dt} \equiv \frac{\partial}{\partial t} + \frac{U_0}{r\cos\phi}\frac{\partial}{\partial \lambda} + \frac{V_0}{r}\frac{\partial}{\partial \phi}. \tag{6.62}$$

The first step is to implement a semi-Lagrangian treatment of the advection and a semi-implicit treatment of the wind perturbation in the Coriolis terms. We write the semi-discrete equations

$$\delta u_a^{n+1} = \delta u_d^n + (1-\alpha_5)\Delta t f \delta v_d^n + \alpha_5 \Delta t f \delta v_a^{n+1}, \tag{6.63}$$

$$\delta v_a^{n+1} = \delta v_d^n - (1-\alpha_5)\Delta t f \delta u_d^n - \alpha_5 \Delta t f \delta u_a^{n+1}, \tag{6.64}$$

where subscript d indicates a value at the departure point, subscript a indicates a value at the arrival point, α_5 is a time-weighting coefficient and Δt is the model time step. We note that we have not yet fixed the position on the grid at which f is calculated. Substituting for δv_a^{n+1} in (6.63) from (6.64) and for δu_a^{n+1} in (6.64) from (6.63) we obtain

$$\delta u_a^{n+1} = s$$

where $E = \exp(i\omega\Delta t)$, $E' = \exp(i(U_0 k\Delta x + V_0 l\Delta y))$. Then a necessary condition for stability is that the modulus of E be less than one. Following Section 2.2.4 we set the determinant of the matrix to zero to obtain the discrete dispersion relation

$$EE' = W_1 \pm iW_2. \tag{6.69}$$

Since $\| E' \| = 1$ we find that

$$\begin{aligned} \| E \|^2 &= W_1^2 + W_2^2 \\ &= \frac{(1 - \alpha_5(1 - \alpha_5)\beta^2)^2 + \beta^2}{(1 + \alpha_5^2\beta^2)^2}. \end{aligned} \tag{6.70}$$

This expression is difficult to analyse in the general case. However, we can obtain the following results for specific cases:

- For $\alpha_5 = 0.5$ we have $\| E \| = 1$ and the scheme is unconditionally stable.
- For $\alpha_5 = 1$ we have

zFsqes ffk[[[[zsq=1xNff)))k qwx“s fl’k[[[sqer,x zN [illegible]

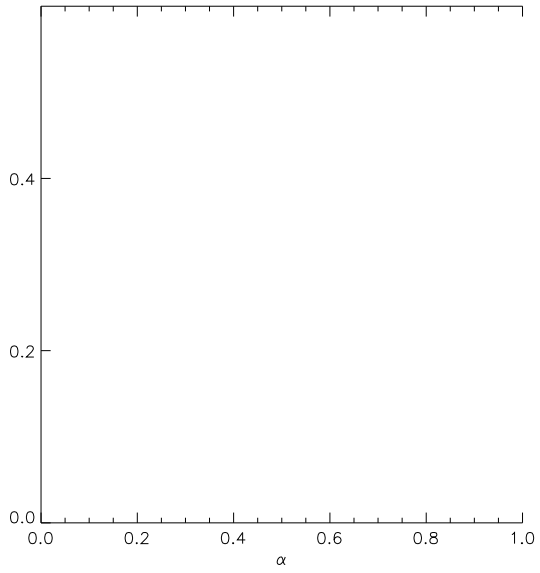
0.4
0.2
0.0
0.0
0.2
0.4
0.6
0.8
1.0
α

$$
\begin{aligned}
\delta\tilde{v} &= W_1\delta v^n_{dv} - \delta v^n - W_2\overline{\delta u}^{\lambda\phi^n}_{dv} - \Delta t\left[(\boldsymbol{\delta u}.\nabla v) + \left(\frac{\overline{\delta u}^{\lambda\phi}\overline{u}^{\lambda\phi}\tan\phi}{\overline{r}^{\phi}}\right)\right] \\
&- \Delta t\Bigg(\left[(1-\alpha_3)\frac{c_p}{\overline{r}^{\phi}}\left(\overline{\theta}^{r\phi}\partial_\phi\delta\Pi - \overline{\theta\partial_r\delta\Pi}^{r\phi}\partial_\phi r\right)\right. \\
&+ \left.(1-\alpha_3)\frac{c_p}{\overline{r}^{\phi}}\left(\overline{\delta\theta}^{r\phi}\partial_\phi\Pi - \overline{\delta\theta\partial_r\Pi}^{r\phi}\partial_\phi r\right)\right]_{dv} \\
&+ \alpha_3\frac{c_p}{\overline{r}^{\phi}}\left(\overline{\theta}^{r\phi}\partial_\phi\delta\Pi - \overline{\theta\partial_r\delta\Pi}^{r\phi}\partial_\phi r\right) \\
&+ \alpha_3\frac{c_p}{\overline{r}^{\phi}}\left(\overline{\delta\theta}^{r\phi}\partial_\phi\Pi - \overline{\delta\theta\partial_r\Pi}^{r\phi}\partial_\phi r\right)\Bigg); \qquad (6.72)
\end{aligned}
$$

$$
\delta\tilde{w} = -\Delta t\left[c_p\delta\theta\partial_r\Pi + c_p\theta\partial_r\delta\Pi\right]. \qquad (6.73)
$$

For the thermodynamic equation we implement a semi-Lagrangian scheme which is non-in

We also have the remaining component of $\boldsymbol{\delta\tilde{\mathbf{x}}}$,

$$\delta\tilde{\Pi} = 0, \tag{6.78}$$

since there is no predictor step for the pressure perturbation.

Computation of $\mathbf{M}^{-1}\boldsymbol{\delta\tilde{\mathbf{x}}}$

The prediction step leaves us with the matrix equation $\mathbf{M}\boldsymbol{\delta}\mathbf{x}' = \boldsymbol{\delta\tilde{\mathbf{x}}}$, given by the equations

$$\begin{aligned} \delta u' &+ \frac{\alpha_3 c_p \Delta t}{\overline{r}^{\lambda}\cos\phi}\left(\overline{\delta\theta'}^{r\lambda}\partial_\lambda\Pi - \overline{\delta\theta'\partial_r\Pi}^{r\lambda}\partial_\lambda r\right) \\ &+ \frac{\alpha_3 c_p \Delta t}{\overline{r}^{\lambda}\cos\phi}\left(\overline{\theta}^{r\lambda}\partial_\lambda\delta\Pi' - \overline{\theta\partial_r\delta\Pi'}^{r\lambda}\partial_\lambda r\right) = \delta\tilde{u}; \end{aligned} \tag{6.79}$$

$$\begin{aligned} \delta v' &+ \frac{\alpha_3 c_p \Delta t}{\overline{r}^{\phi}}\left(\overline{\delta\theta'}^{r\phi}\partial_\phi\Pi - \overline{\delta\theta'\partial_r\Pi}^{r\phi}\partial_\phi r\right) \\ &+ \frac{\alpha_3 c_p \Delta t}{\overline{r}^{\phi}}\left(\overline{\theta}^{r\phi}\partial_\phi\delta\Pi' - \overline{\theta\partial_r\delta\Pi'}^{r\phi}\partial_\phi r\right) = \delta\tilde{v}; \end{aligned} \tag{6.80}$$

$$\delta w' + \Delta t\left[\alpha_4 c_p\delta\theta'\partial_r\Pi + \alpha_4 c_p\theta\partial_r\delta\Pi'\right] = \delta\tilde{w}; \tag{6.81}$$

$$\delta\theta' + \alpha_2\Delta t\partial_{2r}\theta\delta w' = \delta\tilde{\theta}; \tag{6.82}$$

$$\begin{aligned} \delta\rho' &+ \frac{\Delta t}{\partial_\eta r}\left(\frac{1}{\cos\phi}\partial_\lambda\left(\frac{\overline{\rho\partial_\eta r}^{\lambda}}{\overline{r}^{\lambda}}\delta u_1{}'\right) + \frac{1}{\cos\phi}\partial_\phi\left(\frac{\overline{\rho\partial_\eta r}^{\phi}\cos\phi}{\overline{r}^{\phi}}\delta v_1{}'\right)\right. \\ &+ \left.\partial_\eta\left(\overline{\rho}^{r}\partial_\eta r\delta\dot{\eta}_1{}'\right)\right) = \delta\tilde{\rho}; \end{aligned} \tag{6.83}$$

$$\frac{(\kappa-1)\rho\overline{\theta}^{r}p}{\kappa\Pi}\delta\Pi' + p\rho\overline{\delta\theta'}^{r} + p\overline{\theta}^{r}\delta\rho' = 0, \tag{6.84}$$

with

$$\delta u_1{}' = \alpha_1\delta u', \tag{6.85}$$

$$\delta v_1{}' = \alpha_1\delta v', \tag{6.86}$$

$$\delta w_1{}' = \alpha_2\delta w' \tag{6.87}$$

and

$$\delta\dot{\eta}_1{}' - \frac{1}{\partial_\eta r}\left[\delta w_1{}'' - \overline{\frac{\overline{\delta u_1{}'}^{\eta}}{\overline{r}}}\right.$$

and

$$G = 1 - \alpha_2 \alpha_4 c_p \Delta t^2 \partial_{2r} \theta \partial_r \Pi. \tag{6.96}$$

In order to understand better the matrix structure of the equations, we rewrite this

$$G\delta w' + \alpha_4 c_p \Delta t \theta \partial_r \delta \Pi' = \delta w^*. \tag{6.97}$$

The matrix **M** referred to in Section 6.2.2 is given by the left hand sides of (6.79), (6.80), (6.82), (6.84), (6.93) and (6.97). We note that for the w' equation it is the finite difference form of (6.97) that we actually use and not (6.81). This distinction is important, since the above substitution has been made with the analytical equations.

By replacing the horizontal momentum equations with the equations (6.91),

same as that in the nonlinear model, thus allowing the same Fortran code to be used. Having solved (6.98) for $\delta\hat{\Pi}'$ we set $\delta\Pi' = \delta\hat{\Pi}'$.

Final update step

The perturbation xner pressure is updated with

$$\delta\Pi^{n+1} = \delta\Pi^n + \delta\Pi'. \tag{6.99}$$

The perturbation pressure δp can then be updated using (6.26). To find the other components of $\boldsymbol{\delta}\mathbf{x}^{n+1}$ we back substitute into the equations (6.91), (6.92), (6.82), (6.93) and (6.97). We note that by using the approximate equations (6.91) and (6.92) rather than the original equations (6.79) and (6.80) we are updating using the approximate matrix $\mathbf{M_1}$. Finally the values of the perturbation fields at time level $n+1$ are found by adding the increments on to the time level n values.

6.3 Numerical experiments

Having derived the perturbation forecast model it is necessary to validate the model we have coded. This consists of two steps. The first is to check that the code correctly solves the scheme we have set out above. The second step is to check that the model we have developed represents the evolution of a perturbation to sufficient accuracy, that is the validity of the model as defined by Definition 3.3. As we saw for the shallow water model in Section 5.4.2, testing a perturbation forecast model is much more difficult than testing a tangent linear model, since the model is not correct in the sense of Definition 3.2, that is it is not equal to the first order part of the discrete nonlinear model. Hence error measures such as the relative error do not tend to zero with smaller perturbations. In order to make some effort at checking the code, individual subroutines representing the calculation of the various equations are tested by feeding in data for which it is possible to obtain an analytical solution

and chec

perturbations do not provide a realistic test of a linear model. We seek a method of producing initial perturbation fields which have realistic spatial correlations and also realistic inter-correlations between different variables.

The method we use to obtain our initial conditions is described with reference to Figure 6.2. We first take two analyses 24 hours apart, each valid at midnight. We refer to these as analyses valid on Day 0 and Day 1. During the period in which these tests have been carried out the nonlinear model w

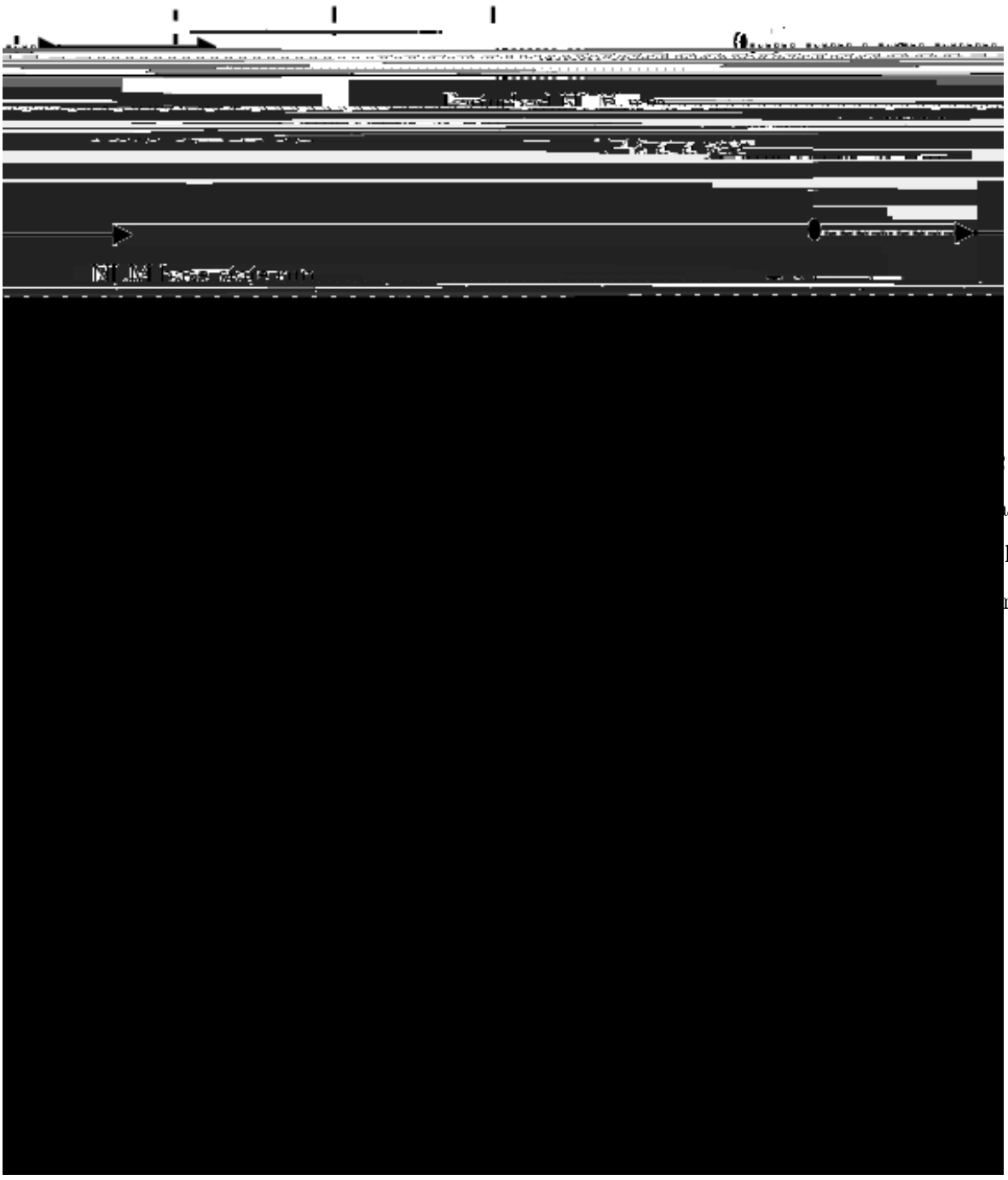

4 and
rrows
line is
ments.

occurs between values of $\alpha = 1.0$ and $\alpha = 0.1$, we also include experiments with the intermediate values 0.5 and 0.2.

The change of relative error with α

Area—weighted r

Thus it appears that the asymptotic values of the graphs plotted cannot give any general information about the performance of the model. In order to assess that the perturbation forecast model is performing satisfactorily we therefore require some other criterion with which to measure its validity. In the following sections we make use of the formulae which we proposed in Section 3.3 in order to provide such a criterion.

6.3.3 Error measures

In order to assess the validity of the perturbation forecast model it is useful to know how much of the linearization error we see is due to nonlinear effects and how much is due to the fact that we have not linearized the discrete nonlinear model. For our three-dimensional model we can make use of the method we derived in Section 3.3 and tested for the shallow water model in Section 5.6. We estimate the linearization error we would expect from a tangent linear model by running the nonlinear model from three different initial conditions and using the formula (3.32) to calculate the estimated tangent linear model (TLM) linearization error $\boldsymbol{\mathcal{E}}$. This can then be compared with the actual linearization error $\mathbf{E}$ from the perturbation forecast model (PFM), found from the difference between the perturbation as evolved in the nonlinear model and the PFM solution.

First we must find a suitable value of the parameter γ to use in the linearization error estimate (3.32). To do this we apply the method suggested in Section 5.6 and plot the evolution of the estimated tangent linear model solution error $\hat{E}_S$ given by

$$\hat{E}_S = 100 \frac{rms(\boldsymbol{\mathcal{E}}^n)}{rms(\boldsymbol{N}^n[\boldsymbol{\delta}\mathbf{U^0}])}, \tag{6.100}$$

for different values of γ.

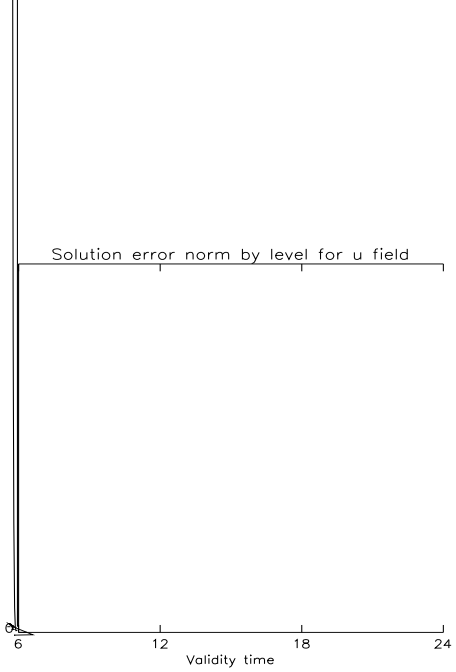
Solution error norm by level for u field
6
12
18
24
Validity time

these fields.

Of particular in

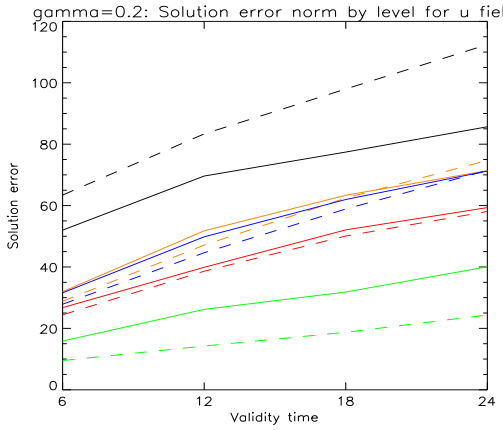
gamma=0.2: Solution error norm by level for u field
Solution error
Validity time
0
20
40
60
80
100
120
6
12
18
24

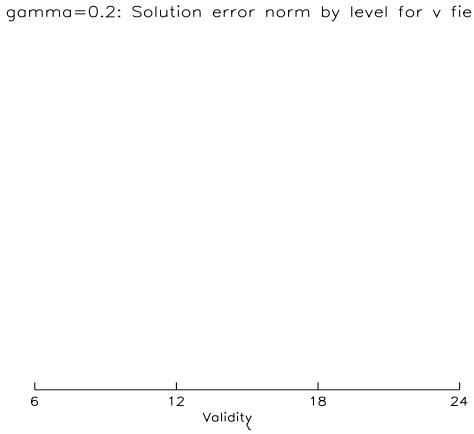
gamma=0.2: Solution error norm by level for v field
6
12
18
24
Validity

Area weighted correlation between levels: u field

From our investigations of different error measures in Section 3.1.2, a good correlation coefficient but high solution error would imply that the linear model is predicting the same pattern of perturbations as the nonlinear model, but that the amplitudes are incorrect. To determine if this is the case we define a damping coefficient C_D by

$$C_D = \frac{rms(\mathbf{L}(t_n, t_0)\boldsymbol{\delta}\mathbf{U^0})}{rms(\boldsymbol{N}^n[\boldsymbol{\delta}\mathbf{U^0}])}. \tag{6.103}$$

Thus for values of $C_D < 1$ the perturbation forecast model field is damped with respect to the nonlinear perturbation. We plot this coefficient for each field in Figure 6.7. It is evident that for all fields except δw the perturbation forecast model is damping with respect to the nonlinear model. The damping is particularly strong for δp between level 12 and 15, but is also present for δu and δv around level 15 and for the other fields slightly higher. For the δw field we have an amplification in the perturbation forecast model with respect to the nonlinear evolution. However, we expect this field to be particularly sensitive to the lack of a friction scheme in the linear model in areas of steep orography. Hence we leave investigation of this field until such a scheme has been implemented. We concentrate our attention on the other fields and now look at the perturbation fields themselves.

6.3.4 Perturbation fields

In this section we continue to look at the fields at validity time T+12 and concentrate our attention on model level 15. This level is chosen for two reasons. Firstly, we have seen from Figure 6.7 that this is the level at which the heaviest damping occurs for the pressure and horizontal wind fields. Secondly, this level is at approximately $500hPa$, which is a level used in other studies we shall compare with. We begin rizone

D

temperature field on level 15 at T+12. From Figure 6.5 we see that the actual PFM and estimated TLM solution errors agree very well for this field and Figure 6.6 shows that the correlation coefficient exceeds 0.94. We show a comparison of the nonlinear and linear perturbations in Figure 6.8. In this figure Plot A shows the perturbation predicted by the nonlinear model, Plot B the perturbation predicted by the perturbation forecast model, Plot C the difference between these and Plot D the estimated TLM linearization error calculated from our formula (3.32). It is clear first of all that the general pattern of the perturbations is the same in the linear and nonlinear models. A comparison of plots C and D shows that in general where there are linearization errors in the perturbation forecast model these also appear in our estimate of the TLM linearization error. The RMS value of the PFM linearization error is 0.53 compared with 0.54 for the estimated TLM error. Thus we see that the error arising from the use of a perturbation forecast model is no greater than that which would be expected with a tangent linear model. We conclude that for this field the main differences between the linear and nonlinear perturbations are due to nonlinear effects rather than approximations in the linear model. The similarity between plots C and D in both pattern and magnitude also reinforces the confidence we have in our error estimate with the chosen parameter.

We now consider the perturbations to pressure at T+12. We note however that because of the choice of grid, level 15 for p is staggered from level 15 for θ. We found in Section 6.3.3 that at this level there was a good correlation between the linear and nonlinear perturbations but a high level of damping in the linear model. Figure 6.9 shows the perturbation fields for this level. Again we plot the nonlinear perturbation, the linear model perturbation, the true PFM linearization error and the estimated TLM linearization error. It is immediately noticeable that

A: N

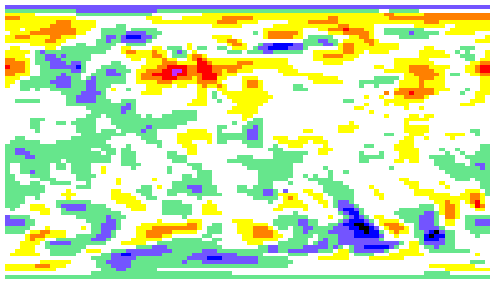

A: Nonlinear perturbation field
Pressure on level 15 at T+ 12
180

A: Nonlinear perturbation f

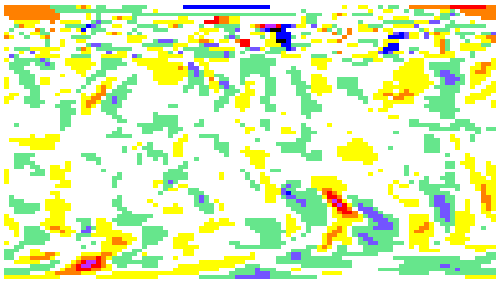

in the perturbations. For the purpose of this study we define the tendency field to be the perturbation field after one time step minus the initial perturbation and do not normalize by the time step. A comparison of this change in the nonlinear and perturbation forecast models allows a judgement to be made as to whether the linear model is changing the initial fields in the correct way.

Before looking at the tendencies it would be useful if we had some estimate of the error we would expect in the tendencies if we had an exact tangent linear model, in a similar way to the error estimate we produced for the fields themselves. We outline a method of achieving this. We suppose that we have an initial perturbation $\boldsymbol{\delta}\mathbf{U^0}$ at time t_0. Now let the nonlinear perturbation after one time step be written $\boldsymbol{N}^{\Delta t}[\boldsymbol{\delta}\mathbf{U^0}]$ and the linear model perturbation be written $\mathbf{L}$

lev

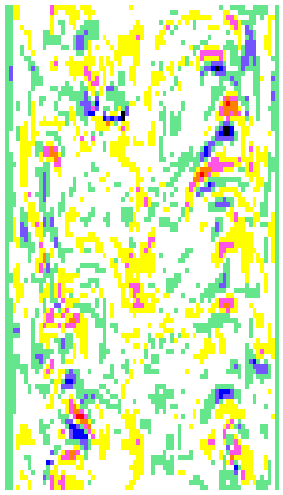

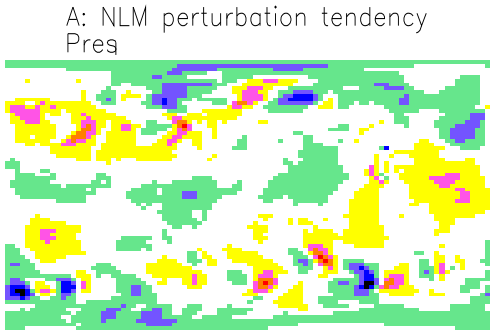
A: NLM perturbation tendency
Pres

case chosen, we have also run from another set of data, changing from a Northern Hemisphere winter to a Northern Hemisphere summer period, July 1999. The initial data were produced in the same way as described in Section 6.3.1. For this case the levels were set up differently and so we have that level 14 is the top of the boundary layer, level 19 is at $500hPa$, level 27 is at $250hPa$ and the first constant height level is level 35. We plot the damping coefficient (6.103) for this case in Figure 6.13. A comparison with Figure 6.7 on page 187 shows that for this case the perturbations from the linear model are damped in a similar way to the December 1998 case. Again we see a large damping of pressure, which is worst between the boundary layer top and $500hPa$, and a damping of the u and v perturbations, peaking slightly higher than $500hPa$. A look at the fields themselves also reveals a similar behaviour to those of the December 1998 case (not shown). Thus we find that the damping for both cases follows the same pattern and even though the model levels are set up differently for the two experiments, the damping peaks at approximately the same pressure level.

Since the damping does not seem to be dependent on the data we must assume that it is caused by a difference between the sc

em

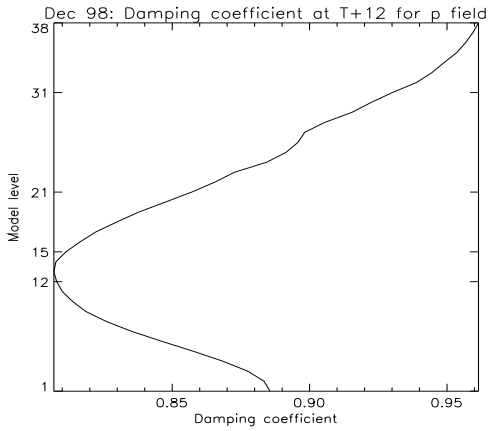

Figure 6.14: Damping coefficient (6.103) for δp plotted against model level for each model field for the December 1998 case with a $900s$ time step.

the linear model could contribute to the difference in amplitude between the linear and nonlinear perturbations.

Ideally we would like to test the effect of truncation error on our results by running the experiment with a different time step and a different spatial resolution such that the ratio of the spatial and temporal steps remains constant. For the three-dimensional model this is not yet possible, since we do not have facilities to change spatial resolution easily. To give some kind of insight as to whether the truncation error may be the source of the damping problem we run the linear model using half the original time step ($900s$), but keeping the spatial resolution as before. The nonlinear model is run with the original $1800s$ time step and so the linearization state in the linear model is only updated every $1800s$ or two time steps. This avoids the extra complication as to the effect of a change in linearization state. In Figure 6.14 we plot the damping coefficient (6.103) for the pressure perturbation for this run, using the data from December 1998. A comparison with the corresponding plot for the run with an $1800s$ time step in Figure 6.7 shows that the variation of damping with height is unchanged. However the minimum value of the damping coefficient has been changed from 0.65 in the $1800s$ time step run to over 0.8 in the

900s time step run, with the damping reduced at all other levels. Plots for other variables show a similar reduction of the damping. Thus we see that running with a smaller time step results in a much more accurate prediction of the amplitude of the perturbations. Although this does not provide a strict test of truncation error, since the spatial resolution remains constant, it does provide some evidence that the amplitude errors are caused by our first order treatment of these extra terms. We outline in Section 7.2 how we propose to investigate this hypothesis further.

6.4 Linearization state

In each of the above experiments we have taken the nonlinear base state to be at the start of the time step, time level n. We have shown in Section 5.5 that in general this will be only first order in time, whereas averaging the linearization state to the centre of the time step for the forcing terms will be second order in time. However, in the three-dimensional perturbation forecast model we are treating the extra term arising from the linearization of advection $(\boldsymbol{\delta}\mathbf{u}.\nabla)$ as in the shallow water model PFM2 of Section 5.2.4, which we found in Section 5.3.3 to be always first order in time. Thus for our three-dimensional model we do not expect any extra accuracy from averaging the linearization state to the centre of the time step.

In order to test this we ran again the experiment described in Section 6.3, but with the linearization state taken to be the average of the time level n and time level $n+1$ values. The control run with which we compare is the run described above with the nonlinear base state taken at time level n. We summarize the results in Table 6.2. In this table we show for each variable the maximum absolute difference between the new perturbation forecast model run and the control (Column A), the model level on which this difference occurs (Column B) and the maximum absolute PFM linearization error on this level (Column C). For each of the variables we find that the maximum change from averaging the nonlinear base state is less than 10%

of the maximum linearization error. We conclude that for this particular model the more accurate linearization state does not have a significant impact, as expected from the theory. However, a greater sensitivity to the linearization state may be found if we were to replace the present first order scheme with one which is second order.

	A	B	C
Field	Maximum absolute difference	Level	Maximum absolute linearization error
δu	4.5 ms^{-1}	3	78.6 ms^{-1}
δv	3.8 ms^{-1}	2	62.7 ms^{-1}
δw	0.05 ms^{-1}	15	1.75 ms^{-1}
δp	49.8 Pa	1	1530 Pa
$\delta \rho$	0.01 kgm^{-3}	1	0.32 kgm^{-3}
$\delta \theta$	3.5 K	1	48.0 K

Table 6.2: Comparison of difference between run of the perturbation forecast model with the nonlinear base state at the start and the centre of the time step. Column A shows the maximum absolute difference between the fields, Column B shows on what level this difference occurs and Column C shows the maximum PFM linearization error from the control run on this level.

6.5 Summary

In this chapter we have applied the semi-continuous method to derive the linearization of a full three-dimensional numerical weather prediction model. In doing so we have made use of the study of the shallow water model in Chapter 5 to help validate our results. Firstly tdlnroyaw)fqIx'qhapterxN =))e

arising from the linearization of advection. In the three-dimensional model of this chapter we treated this term at the arrival poin

are encouraging. As for the simple models developed in Chapters 4 and 5, we have found for the three-dimensional model that the linear model developed using the semi-continuous method is able to predict the approximate evolution of a perturbation. For some of the fields we have validated this prediction was as accurate as that which we would expect from a tangent linear model, even for a 24 hour forecast. This was particularly true for perturbations to the horizontal wind components and the potential temperature away from the model boundaries. We expect that with considered modifications of the numerical scheme this accuracy could also be achieved for the other fields. We discuss some further ideas for achieving this in Section 7.2.

Chap er 7

Conclusions an u ure work

In Chapter 3 we posed the question "Can the semi-continuous method provide us with a linear model which is as accurate as the tangent linear model formed by the discrete method while avoiding some of the problems associated with linearizing discrete numerical models?" We now summarize the results we have found which begin to answer this question and discuss some ideas for further work.

7.1 Summary of results

In examining the linear model formed by the semi-continuous method we have considered its accuracy from three different perspectives which we defined in Chapters 2 and 3. These are truncation error, correctness and validity. For the ordinary differential problem of Chapter 4 it was also possible to examine the linear stability of the models.

We have seen that the linear model is 'correct', as defined by Definition 3.2, if it is formed by the discrete method, whereas the perturbation forecast model formed by the semi-continuous method is not usually correct in this sense. This became more apparent when we looked at a PD problem in Chapter 5, since it is clear that some degree of freedom is available when discretizing the continuous linear equations.

In terms of truncation error, for the examples of the schemes we studied the tangent linear model was found to be as accurate as the discrete nonlinear model from which it is derived. For the perturbation forecast model this is not necessarily the case. The example of the OD problem of Chapter 4 and the shallow water problem of Chapter 5 have shown that the accuracy of the perturbation forecast model may be compromised by two factors, the way in which the numerical scheme is applied and the choice of linearization state. The first of these arises only in the PD problem, again from the freedom with which the linearized equations may be discretized. This was illustrated by the two versions of the perturbation forecast model for the shallow water problem of Chapter 5. We found that two slightly differen

linear models. Nevertheless great care must be taken in the design of a perturbation forecast model to ensure that the accuracy is as good as is required.

7.2 Further work

Having begun to answer the question which we posed, we now consider how this work may be extended in order to provide further insight into the two methods for deriving a linear model. The first extension concerns the shallow water model of Chapter 5. Although the studies of that chapter showed very little difference between the tangent linear model and perturbation forecast model, the experiments we were able to carry out were limited in scope. This was partly due to the fact that it was only possible to find simple problems for the system which were not too highly nonlinear. A useful exercise would be to extend this model to include rotation. Such an extension would allow a greater range of experiments to be run. It would also result in the system having a Rossby mode solution as well as the two gravity modes. This would enable a study of how well the linear models treat a Rossby mode, which could be compared with the results found for the gravity waves.

A second extension of the problem would be to derive the adjoints of the different linear models. We expect the accuracy of the adjoint to be linked to that of the linear model. However it may be that using the adjoints in simple sensitivity or assimilation tests would give a better quantative measure of the difference between the linear models. This would also be a more stringent test of the adjoint model formed via the semi-continuous method, since although the application of incremental four-dimensional variational data assimilation allows an approximate linear model and adjoint, other applications of adjoints require the gradient to be as accurate as possible.

At the same time, it is clear that further work is required on the three-dimensional

model. One problem remaining from this study is the damping effect of our perturbation forecast model which we reported in Chapter 6. We conjectured that this may be due to the treatment of the term arising from the linearization of advection, which we showed in the study of the shallow water model to be first order in time. Although this did not seem to be detrimental to the performance of the simple model it is certainly not desirable to have such an error. The alternative considered in the shallow water model was to average the term along the trajectory, but this holds extra complications for the three-dimensional model since it adds extra coupling between the equations. We therefore require another second order discretization of this term. The scheme we have identified and intend to test is an extrapolation in time at the mid-point of the trajectory, in much the same way as the departure point calculation is performed. Thus, for example in the linearized thermodynamic equation, we would have

$$\delta$$

effect seen in the linear model. However, more work is needed to investigate the comparative stability and accuracy properties of these different schemes.

and R is the vector of components R_i. The iterative procedure proposed to solve this equation is given by equation (5.52) on page 93,

$$\begin{aligned} -C{\phi'_{i+1}}^{(m+1)} &+ \left(2C + \frac{1}{\Phi_{ref}}\right)\phi_i'^{(m+1)} - C{\phi'_{i-1}}^{(m+1)} \\ &= R_i - \ln(\Phi_{ref} + \phi_i'^{(m)}) + \frac{\phi_i'^{(m)}}{\Phi_{ref}}. \end{aligned} \tag{A.5}$$

This is a fixed point iteration which can be written in the form

$$\boldsymbol{\phi}'^{(m+1)} = \mathbf{L}^{-1}(R - N(\boldsymbol{\phi}'^{(m)})). \tag{A.6}$$

In order to show the conditions under which this iteration will converge, we make use of the fixed-point theorem, taken from [62]. We first define a general iteration of the form

$$\mathbf{g}(\mathbf{x}^{(m+1)}, \mathbf{x}^{(m)}) = 0, \qquad m = 0, 1, 2, \ldots \tag{A.7}$$

We denote by $\mathbf{g_x}$ and $\mathbf{g_y}$ the $n \times n$ matrices

$$\mathbf{g_x}(x, y) = \left(\frac{\partial \mathbf{g}_i}{\partial x_j}(x, y)\right), \qquad \mathbf{g_y}(x, y) = \left(\frac{\partial \mathbf{g}_i}{\partial y_j}(x, y)\right). \tag{A.8}$$

We also require the definition of the spectral radius of a matrix:

Definition A.1 *Let* $\mathbf{C}$ *be a matrix with eigenvalues* $\lambda_1, \lambda_2, \ldots, \lambda_n$. *Then the* spectral radius *of* $\mathbf{C}$, *written* $\rho(\mathbf{C})$, *is defined by*

$$\rho(\mathbf{C}) = \max_i |\lambda_i|. \tag{A.9}$$

We then have the following theorem:

Theorem A.1 (Fixed-point theorem) *Let* S' *be an open neighbourhood of a point* $\mathbf{x}^* \in R^n$. *Assume that* $\mathbf{g} \in C^1(S' \times$

In order to apply this theorem to our iteration (A.6) we first note that it can be written in the form (A.7) by defining

$$\mathbf{g}(\boldsymbol{\phi}'^{(m+1)}, \boldsymbol{\phi}'^{(m)}) = \mathbf{L}\boldsymbol{\phi}'^{(m+1)} + N(\boldsymbol{\phi}'^{(}$$

$$_r\,($$

implies that

$\mathbf{D}$ is a diagonal matrix with entries given by (A.14), we find that $\mathbf{L} \pm \mathbf{D}$ is the tridiagonal matrix with entries

$$\left(-C, 2C + \frac{1}{\Phi_{ref}} \pm \frac{1}{\Phi_{ref}}\left(1 - \frac{\Phi_{ref}}{\Phi_{ref} + \phi_i'}\right), -C\right). \tag{A.19}$$

A sufficient condition for this matrix to be symmetric positive definite is that it be strictly diagonally dominant. This will certainly occur if

$$\frac{1}{\Phi_{ref}} \geq \left|\frac{1}{\Phi_{ref}}\left(1 - \frac{\Phi_{ref}}{\Phi_{ref} + \phi_i'}\right)\right|. \tag{A.20}$$

For $\phi_i' > 0$ this condition always holds. For $\phi_i' < 0$ (A.20) holds for

$$|\phi_i'| < \frac{\Phi_{ref}}{2}. \tag{A.21}$$

Hence (A.21) provides a sufficient condition for the convergence of the iteration (A.5).

We note also that from (5.48) we have $\Phi_{ref} + \phi_i{}' = \phi_i^{n+1}$, the value of ϕ_i at the new time level, and so we can write the convergence condition (A.20) as

$$\frac{1}{\Phi_{ref}} \geq \left|\frac{1}{\Phi_{ref}}\left(1 - \frac{\Phi_{ref}}{\phi_i^{n+1}}\right)\right|. \tag{A.22}$$

Hence a sufficient condition for convergence is that $\Phi_{ref} < \phi_i^{n+1}$. We can therefore guarantee convergence by choosing a value of Φ_{ref} less than any expected value of ϕ_i at the new time level.

Appendix B

Helmholtz equation for 3-dimensional model

The Helmholtz equation for the perturbation forecast model resulting from substitution into (6.98) takes the following form:

$$\begin{aligned} &\frac{1}{\cos\phi}\partial_\lambda\left(C_{xx1}X\right)+\frac{1}{\cos\phi}\partial_\phi\left(C_{yy1}Y\right) \\ &+\partial_\eta\left[C_{zz}\delta_\eta\delta\hat{\Pi}'-C_5\left(\overline{C_{xz}\overline{X}^{\eta}}^{\lambda}+\overline{C_{yz}\overline{Y}^{\eta}}^{\phi}\right)\right] \\ &+C_3\left[\overline{C_z\partial_\eta\delta\hat{\Pi}'}^{r}\right] \\ &-C_4\delta\hat{\Pi}' \;=\; RHS, \end{aligned} \tag{B.1}$$

with X and Y are defined by

$$X=C_{xx2}\left(\partial_\lambda\delta\hat{\Pi}'-C_{xp}\overline{C_2\partial_r\delta\hat{\Pi}'}^{r\lambda}\right), \tag{B.2}$$

$$Y=C_{yy2}\left(\partial_\phi\delta\hat{\Pi}'-C_{yp}\overline{C_2\partial_r\delta\hat{\Pi}'}^{r\phi}\right), \tag{B.3}$$

and the notation following that introduced on Page 160. The coefficients are given by

$$C_{xx1}=\frac{\overline{\rho\partial_\eta r}^{\lambda}}{\overline{r}^{\lambda}}, \tag{B.4}$$

$$C_{xx2} = \frac{\alpha_1\alpha_3\Delta t c_p \overline{\theta}^{r\lambda}}{\overline{r}^{\lambda}\cos\phi}, \tag{B.5}$$

$$C_{yy1} = \frac{\overline{\rho\partial_\eta r}^{\phi}\cos\phi}{\overline{r}^{\phi}}, \tag{B.6}$$

$$C_{yy2} = \frac{\alpha_1\alpha_3\Delta t c_p \overline{\theta}^{r\phi}}{\overline{r}^{\phi}}, \tag{B.7}$$

$$C_{zz} = \frac{\alpha_2\alpha_4 c_p \Delta t \overline{\rho}^{r}\theta}{\partial_\eta r G}, \tag{B.8}$$

$$C_{z} = \frac{\alpha_2\alpha_4 c_p \Delta t \theta\partial_{2r}\theta}{\partial_\eta r G}, \tag{B.9}$$

$$C_{xz} = \frac{\partial_\lambda r}{\overline{r}^{\lambda}\cos\phi}, \tag{B.10}$$

$$C_{yz} = \frac{\partial_\phi r}{\overline{r}^{\phi}}, \tag{B.11}$$

$$C_{xp} = \frac{\partial_\lambda r}{\overline{\theta}^{r\lambda}}, \tag{B.12}$$

$$C_{yp} = \frac{\partial_\phi r}{\overline{\theta}^{r\phi}}, \tag{B.13}$$

$$C_{2} = \theta, \tag{B.14}$$

$$C_{3} = \frac{\rho\partial_\eta r}{\overline{\theta}^{r}}, \tag{B.15}$$

$$C_{4} = \frac{(1-\kappa)\rho\partial_\eta r}{\kappa\Pi\Delta t}, \tag{B.16}$$

$$C_{5} = \overline{\rho}^{r}, \tag{B.17}$$

$$\begin{aligned} RHS &= \frac{\partial_\eta r}{p\theta\Delta t}\Bigg(- p\rho\overline{\Big(\delta\tilde{\theta} - \frac{\alpha_2\Delta t\partial_{2r}\theta}{G}\delta w^*\Big)}^{r} - p\theta\delta\tilde{\rho}\Bigg) \\ &+ \frac{1}{\cos\phi}\partial_\lambda\Bigg(\alpha_1\frac{\overline{\rho\partial_\eta r}^{\lambda}}{\overline{r}^{\lambda}}\delta u^*\Bigg) + \frac{1}{\cos\phi}\partial_\phi\Bigg(\alpha_1\frac{\overline{\rho\partial_\eta r}^{\phi}}{\overline{r}^{\phi}}\cos\phi\delta v^*\Bigg) \\ &+ \partial_\eta\Bigg(\overline{\rho}^{r}\Big(\frac{\alpha_2\delta w^*}{G} - \frac{\overline{\alpha_1\overline{\delta u^*}^{\eta}}^{\lambda}}{\overline{r}^{\lambda}\cos\phi}\partial_\lambda r - \frac{\overline{\alpha_1\overline{\delta v^*}^{\eta}}^{\phi}}{\overline{r}^{\phi}}\partial_\phi r\Big)\Bigg). \end{aligned} \tag{B.18}$$

Bibliography

[1] W.K. Anderson and V. Venkatakrishan. Aerodynamic design optimization on unstructured grids with a continuous adjoint formulation. *Computers and Fluids*, 28:443–480, 1999.

[2] J-W. Bao and Y-H. Kuo. On/off switches in the adjoint method: Step functions. *Mon. Wea. Rev.*, 123:1589–1594, 1995.

[3] J-W. Bao and T.T. Warner. Treatment of on/off switches in the adjoint method: FDDA experiments with a simple model. *Tellus*, 45A:525–538, 1993.

[4] M.C. Bartholomew-Biggs. Using forward accumulation for automatic differentiation of implicitly-defined functions. *Computational Optimization and Applications*, 9:65–84, 1998.

[5] M.C. Bartholomew-Biggs, S. Brown, B. Christianson, and L. Dixon. Automatic differentiation of algorithms. *Journal of Computational and Applied Mathematics*, 124:171–190, 2000.

[6] G.K. Batchelor. *An introduction to fluid dynamics.* Cambridge University Press, 1967.

[7] F.H.M. Bates, J.R. Semazzi and R.W. Higgins. Integration of the shallow water equations on the sphere using a vector semi-Lagrangian scheme with a multigrid solver. *Mon. Wea. Rev.*, 118:1615–1627, 1990.

[8] J.R. Bates, S. Moorthi, and R.W. Higgins. A global multilev

[17] P. Courtier, J-N. Thepaut, and A. Hollingsworth. A strategy for operational implementation of 4D-Var, using an incremental approach. *Quart. J. Roy. Meteor. Soc.*, 120:1367–1387, 1994.

[18] M.J.P. Cullen, T. Davies, M.H. Mawson, J.A. James, S.C. Coulter, and A. Malcolm. An overview of numerical methods for the next generation U.K. NWP and climate model. In C.A. Lin, R. Laprise, and H. Ritchie, editors, *Numerical methods in atmospheric and oceanic modelling*, pages 425–444. Canadian

[26] R.M. rrico and K.D. Raeder. An examination of the accuracy of the linearization of a mesoscale model with moist physics. *Quart. J. Roy. Meteor. Soc.*, 125:169–195, 1999.

[27] R.M. rrico and T. Vukićević. Sensitivity analysis using an adjoint of the PSU-NCAR mesoscale model. *Mon. Wea. Rev.*, 120:1644–1660, 1992.

[28] R.M. rrico, T. Vukićević, and K. Raeder. xamination of the accuracy of a tangent linear model. *Tellus*, 45A:462–477, 1993.

[29] A.J. Gadd. Two refinements of the split explicit integration scheme. *Quart. J. Roy. Meteor. Soc.*, 106:215–220, 1980.

[30] C.W. Gear. *Numerical initial value problems in ordinary differential equations.* Prentice-Hall, 1971.

[31] M. Ghil and P. Malanotte-Rizzooli. Data assimilation in meteorology and oceanography. *Advances in Geophysics*, 33:141–266, 1991.

[32] R. Giering and T. Kaminski. Recipes for adjoint code construction. *ACM Trans. On Math. Software*, 24:437–474, 1998.

[33] M.B. Giles and N.A. Pierce. An introduction to the adjoint approach to design. *European Journal of Flow, Turbulence and Combustion*, 2000. To appear.

[34] A. Griewank. On automatic differentiation. In Iri and Tanabe [47], pages 83–108.

[35] A. Griewank, C. Bischof, G. Corliss, A. Carle, and K. Williamson. Derivative convergence for iterative equation solvers. *Optimization Methods and Software*, 2:321–355, 1993.

[36] N.J. Higham. Stable iterations for the matrix square root. *Numerical Algorithms*, 15:227–242, 1997.

[37] M. Hortal. The development and testing of a new two-time-level semi-Lagrangian scheme (S TTLS) in the CMWF forecast model. *Quart. J. Roy. Meteor. Soc.*, 1999. Submitted.

[38] D.D. Houghton and A. Kasahara. Nonlinear shallow fluid flow over an isolated ridge. *Comm. Pure Appl. Math.*, 21:1–23, 1968.

[39] N.B. Ingleby. The statistical structure of forecast errors and its representation in the Met Office global 3-dimensional variational data assimilation scheme. *Quart. J. Roy. Meteor. Soc.*, 2001. To appear.

[40] A. Jameson, N. Pierce, and L. Martinelli. Optimum aerodynamic design using the Navier-Stokes equations. *J. Theor. Comp. Fluid Mech.*, 10:213–237, 1998.

[41] M. Janiskova, J-N. Thepaut, and J-F. Geleyn. Simplified and regular physical parametrizations for incremental four-dimensional variational assimilation. *Mon. Wea. Rev.*, 127:26–45, 1999.

[42] H. Kreiss and J. Oliger. *Methods for the approximate solution of time dependent problems.* Number 10 in GARP publications series. World Meterological Organization, 1973.

[43] K. Krishna. Commutativity of differentiation and discretization with special reference to finite element and finite difference discretizations. *Numer. Funct. Anal. and Optimiz.*, 7:235–265, 1984.

[44] J.D. Lambert. *Computational methods in Ordinary Differential Equations.* John Wiley and Sons, 1973.

[45] J.D. Lambert. *Numerical methods for Ormetho*

[46] A.S. Lawless and N.K. Nichols. A comparison of two methods of deriving the tangent linear model. Forecasting Research Technical Report 257, The Met Office, 1998.

[47] F.-X. Le Dimet, editor. *High-performance computing in the geosciences.* Kluwer Academic Publishers, Boston, Mass., 1995.

[48] F-X. Le Dimet and O. Talagrand. Variational algorithms for analysis and assimilation of meteorological observations: theoretical aspects. *Tellus*, 38A:97–110, 1986.

[49] Y. Li et al. Variational data assimilation with a semi-Lagrangian semi-implicit global shallow-water equation model and its adjoint. *Mon. Wea. Rev.*, 121:1759–1769, 1993.

[50] Y. Li et al. Four-dimensional variational data assimilation experiments with a multilevel semi-Lagrangian semi-implicit general circulation model. *Mon. Wea. Rev.*, 122:966–983, 1994.

[51] A. Lorenc. Analysis methods for numerical weather prediction. *Quart. J. Roy. Meteor. Soc.*, 112:1177–1194, 1986.

[52] P. Lynch. Richardson's marvellous forecast. pages 61–73. Amer. Met. Soc., Boston, 1999.

[53] A. McDonald. Accuracy of multiply-upstream, semi-Lagrangian advective schemes. *Mon. Wea. Rev.*, 112:1267–1275, 1984.

[54] A. McDonald. Accuracy of multiply-upstream, semi-Lagrangian advective schemes II. *Mon. Wea. Rev.*, 115:1446–1450, 1987.

[55] A. McDonald and J.R. Bates. Impro

[64] S. Polavarapu and M. Tanguay. Linearizing iterative processes for four-dimensional data assimilation sc

[83] C Temperton and Staniforth A. An efficient two-time-level semi-Lagrangian semi-implicit integration scheme. *Quart. J. Roy. Meteor. Soc.*, 113:1025–1039, 1987.

[84] C Temperton, M. Hortal, and A. Simmons. A two-time-level semi-Lagrangian global spectral model. *Quart. J. Roy. Meteor. Soc.*, 1999. Submitted.

[85] J-N. Thepaut and P. Courtier. Four-dimensional variational data assimilation using the adjoint of a multilevel primitive-equation model. *Quart. J. Roy. Meteor. Soc.*, 117:1225–1254, 1991.

[86] J-N. Thepaut, R.N. Hoffman, and P. Courtier. Interactions of dynamics in a four-dimensional variational assimilation. *Mon. Wea. Rev.*, 121:3393–3414, 1993.

[87] J. Thuburn and T.W.N. Haine. Adjoints of nonoscillatory advection schemes. *J. Comput. Phys.*, 2000. Submitted.

[88] T. Vukićević and J-W. Bao. The effect of linearization errors on 4DVAR data assimilation. *Mon. Wea. Rev.*, 126:1695–1706, 1998.

[89] A. Wiin-Nielsen. The birth of numerical weather prediction. *Tellus*, 43AB:36–52, 1991.

[90] Q. Xu. Generalized adjoint for physical processes with parameterized discontinuities. Part I: Basic issues and heuristic examples. *J.A.S.*, 53:1123–1155, 1996.

[91] J. Zhu and M. Kamachi. The role of time step size in numerical stability of tangent linear models. *Mon. Wea. Rev.*, 128:1562–1572, 2000.

[92] X. Zou. Tangent linear and adjoint of 'on-off' proceses and their feasibility for use in 4-dimensional variational data assimilation. *Tellus*, 49A:3–31, 1997.

[93] X. Zou, Y-H. Kuo, and Y-R. Guo. Assimilation of atmospheric radio refractivity using a nonydrostatic adjoint model. *Mon. Wea. Rev.*, 123:2229–2249, 1995.

[94] D. Zupanski and D Mesinger. Four-dimensional variational data assimilation of precipitation data. *Mon. Wea. Rev.*, 123:1112–1125, 1995.

[95] M. Zupanski. Regional four-dimensional variational data assimilation in a quasi-operational forecasting environment. *Mon. Wea. Rev.*, 121:2396–2408, 1993.